

Department of Physics
Faculty of Science
University of Helsinki

SINGLE MOLECULE BIOPHYSICS OF VIRAL GENOME TRANSLOCATION

Kalle Hanhijärvi

ACADEMIC DISSERTATION

To be presented, with the permission of the Faculty of Science of the University of Helsinki, for public examination in auditorium XII of the University of Helsinki main building, Unioninkatu 34, on May 27th 2016, at 12 noon.

Helsinki 2016

Supervisor

Professor Edward Hægström
Department of Physics
University of Helsinki
Finland

Reviewers

Professor Nynke Dekker
Kavli Institute of Nanoscience
Delft University of Technology
The Netherlands

Professor Wouter H. Roos
Zernike Institute for Advanced Materials
University of Groningen
The Netherlands

Opponent

Professor William M. Gelbart
Department of Chemistry and Biochemistry
University of California, Los Angeles
The United States of America

Cover art: Single molecule data of ssRNA packaging by ϕ 16 with an inset schematic

© Kalle Hanhijärvi 2016

Report Series in Physics HU-P-D239

ISBN 978-951-51-1584-3 (paperback)

ISBN 978-951-51-2213-1 (PDF)

ISSN 0356-0961

Unigrafia
Helsinki 2016

ABSTRACT

Viruses are the most abundant form of life on Earth. They cause serious disease, significant suffering, and economic losses, but viruses are also important to the general balance of the ecosystem. Understanding the details of the viral lifecycle is therefore essential from the point of view of basic research. This thesis work expands the basis formed by traditional microbiology. Single molecule biophysics techniques open a unique perspective into the inner workings of viruses. The physics point of view provides a quantitative, predictive, and descriptive mathematical basis to help one understand the basic processes of life. Furthermore, single molecule methods reveal heterogeneity and process variability which are unresolvable in bulk studies.

This thesis work employs single molecule biophysical experiments to study two aspects of the viral lifecycle: genome packaging and ejection.

DNA ejection is a method of infection employed by many double-stranded DNA (dsDNA) bacteriophages. Their viral genome is packaged under high pressure within a small volume comparable in linear dimension to the persistence length of dsDNA. Viruses infecting archaea are a new and emerging field of study, which benefits from the single-molecule perspective. This thesis presents the first single molecule study of dsDNA ejection from an Archaeal virus His1, which has a dsDNA genome packaged in a lemon-shaped capsid. Osmotic suppression experiments are carried out and results are compared to those of established dsDNA phages. Results obtained with total internal reflection fluorescence microscopy indicate that DNA ejection from His1 is modulated by external salt concentration and osmotic pressure as is common to many bacteriophages. These findings qualitatively agree with the predictions given by the continuum theory of dsDNA packaging.

In contrast to DNA ejection, genome packaging is essential to the assembly of virus particles. Here the focus is on *Pseudomonas* phage phi6 which has a three-part dsRNA genome, of which only positive sense ssRNA-segments are packaged into the preformed procapsid. This thesis presents the first optical tweezers experiment of single-stranded RNA (ssRNA) packaging by phi6. The results show that packaging alternates between fast and slow sections suggesting that the secondary structure of the ssRNA segment is opened as the RNA is packaged.

Single molecule-level results obtained using the two model systems reveal previously unseen heterogeneity in the ejection and packaging processes. Such results cannot be obtained by bulk methods alone.

CONTENTS

Abstract.....	3
Contents.....	4
List of original publications.....	6
Abbreviations.....	8
1 Introduction.....	9
1.1 Single molecule biophysics	9
1.2 Genome ejection and packaging.....	10
1.3 Archaeal virus His1	10
1.4 Bacteriophage phi6	12
2 Aims	14
3 Theory	15
3.1 Continuum model of DNA ejection	15
4 Methods	18
4.1 Optical tweezers with fluorescence microscopy.....	18
4.2 Assay preparation	20
4.2.1 His1 ejection assay	20
4.2.2 Phi6 packaging assay.....	21
4.3 Data analysis	22
4.3.1 Fluorescence images	22
4.3.2 Optical tweezers measurements	23
4.3.2.1 Calibration	23
4.3.2.2 Packaging velocity	24
4.3.2.3 Packaging in sections	25
5 Results.....	26

5.1.1	DNA ejection from His1	26
5.1.1.1	Directionality of ejection	27
5.1.1.2	Osmotic suppression experiments.....	28
5.1.1.3	Effect of salts	29
5.1.1.4	Effect of pH	32
5.1.1.5	Effect of temperature	33
5.1.2	Single-stranded RNA packaging of phi6	35
5.1.2.1	Average packaging velocity	35
5.1.2.2	Packaging alternates between fast and slow sections	37
6	Discussion.....	40
6.1	DNA ejection from His1 is suppressed by osmotic pressure and increasing salt concentration.....	40
6.2	DNA ejection from His1 is stable as a function of temperature and pH	41
6.3	RNA packaging of phi6 alternates between fast and slow velocities.....	42
6.4	Conclusions	43
	Acknowledgements	44
	References	45
	Appendix A: His1 capsid dimensions.....	49
	Appendix B: Optical parts of the TIRF microscope.....	50

LIST OF ORIGINAL PUBLICATIONS

This thesis is based on three primary publications:

- I K.J. Hanhijärvi, G. Ziedaite, M.K. Pietilä, E. Hæggström, and D.H. Bamford, *DNA Ejection from an Archaeal Virus – A Single Molecule Approach*, *Biophysical Journal*, 2013. **104**(10): pp. 2264-2272.
doi:10.1016/j.bpj.2013.03.061
- II K.J. Hanhijärvi, G. Ziedaite, E. Hæggström, and D.H. Bamford, *Temperature and pH dependence of DNA ejection from archaeal lemon-shaped virus His1*, Accepted for publication in *European Biophysics Journal*, 2016.
- III K.J. Hanhijärvi, G. Ziedaite, D.H. Bamford, E. Hæggström, and M.M. Poranen, *Single-molecule measurements of viral ssRNA packaging*, submitted for publication, 2016.

These publications are referred to in the text by the Roman numerals (I-III).

Author's contribution

The author designed, constructed, and incorporated the fluorescence illumination and detection systems into the optical tweezers instrument that was used in papers I and II. He carried out all single-molecule experiments, did all the data analysis presented in the papers, and designed the data analysis procedures. The author wrote all papers with G.Z., with an equal contribution.

Additional original publications by the author published during his training

K. Hanhijärvi, T. Majava, I. Kassamakov, J. Heinämäki, J. Aaltonen, J. Haapalainen, E. Hægström and J. Yliruusi, *Scratch Resistance of Plasticized Hydroxypropyl Methylcellulose (HPMC) Films Intended for Tablet Coatings*, European Journal of Pharmaceutics and Biopharmaceutics, 2009, **74**(2), pp. 371-376.

K. Hanhijärvi, I. Kassamakov, V. Heikkinen, J. Aaltonen, L. Sainiemi, K. Grigoras, S. Franssila, and E. Hægström, *Stroboscopic supercontinuum white-light interferometer for MEMS characterization*, Optics Letters, 2012, **37**(10), pp. 1703-1705.

K. Hanhijärvi, I. Kassamakov, J. Aaltonen, V. Heikkinen, L. Sainiemi, S. Franssila, and E. Hægström, *Through-silicon stroboscopic characterization of oscillating MEMS thermal actuator using supercontinuum interferometry*, IEEE/ASME Transactions on Mechatronics, 2009, **8**(4), pp. 1418-1420.

I. Kassamakov, K. Hanhijärvi, I. Abbadi, J. Aaltonen, H. Ludvigsen, and E. Haeggström, *Scanning white light interferometry with a supercontinuum source*, Optics Letters, 2009, **34**(10), pp. 1582-1584.

ABBREVIATIONS

atm	Standard atmosphere (101.325 kPa)
DNA	Deoxyribonucleic acid
ds	Double-stranded
EMCCD	Electron multiplying charge coupled device
kb	Kilo-base pair
nt	Nucleotide
OT	Optical tweezers
PC	Procapsid or polymerase complex
PEG	Polyethylene-glycol
PSD	Position sensitive detector
RNA	Ribonucleic acid
ROI	Region of interest
RT	Room temperature
ss	Single-stranded
TIRF	Total internal reflection fluorescence

Symbols

c	Length-scale parameter of the electrostatic repulsion
d_{capsid}	Time-dependent capsid expansion
d_s	DNA strand separation in hexagonal packaging
F_o	Strength parameter of electrostatic repulsion
f_c	Corner frequency
G_{tot}	Total packaging free energy
k_B	Boltzmann constant
k_j	Trap stiffness in direction j
h	Major axis of an ellipsoid
L	Packaged genome length
$L_{RNA, fold}$	Length of folded ssRNA
$N(R')$	Number of DNA loops at radius R'
R	Inner radius of packaged DNA loop
R'	Radius variable in integration
R_{DNA}	Effective radius of DNA
R_{out}	Outer radius of the capsid in the continuum model
v_{P4}	Packaging velocity of P4
β	Drag coefficient
η	Dynamic viscosity of buffer
ξ_p	Persistence length of dsDNA
Π_o	Osmotic pressure

1 INTRODUCTION

1.1 SINGLE MOLECULE BIOPHYSICS

Single molecule biophysics approaches problems in biosciences from a physics perspective [1]. The aim of physics is to describe and quantify phenomena of the natural world. One particular approach of physics is to describe microscopic scale phenomena that make up the natural world on the larger scale. As an example of this approach, this thesis focuses on viral genome translocation. The physical scale of the world of viruses is small, with lengths in the nanometer-micrometer range and relevant forces in pico- to nanonewtons. Nevertheless, understanding these small scale interactions is important in the larger scale of ecosystems, where viruses play an important part in populations of organisms. The single molecule perspective also provides an important complementary methodology to support research employing bulk methods [2, 3]. Numerous single molecule methods have been developed, and they can be classified into methods of sensing (imaging or detection) and methods of manipulation.

Optical trapping is an established method for micromanipulation and characterization. An optical tweezers (OT) instrument employs a tightly focused laser beam that traps a dielectric particle, usually a glass or plastic sphere, in a liquid medium [4-8]. The laser focus forms a 3D harmonic potential minimum in which the particle is confined. Since the potential is known (harmonic), it is possible to measure the forces acting on the trapped particle in addition to measuring its position. An OT instrument can be used to generate and measure forces up to tens of piconewtons and sub-nanometer displacements [4].

Fluorescence methods are also employed in life sciences since these methods provide sensitive detection and imaging. Fluorescence microscopy is favored for its sensitivity. A single fluorophore can emit hundreds of photons, which are readily detectable [3]. Extending traditional epifluorescence microscopy towards single molecule studies is often limited by one's ability to suppress background fluorescence. Emission from a small number of fluorophores is easily lost in the background of large number of other molecules in typical experimental volumes [9]. This issue can be addressed by using confocal methods or total internal reflection excitation.

This thesis focuses on the single molecule biophysics of two aspects of the viral lifecycle, ejection and packaging. The first part considers DNA ejection from the archaeal virus His1, whereas the second part deals with ssRNA packaging of *Pseudomonas* phage phi6. In addition to being the first single molecule experiments of DNA ejection for an Archaeal virus and OT experiment of dsRNA phage packaging, these two biological systems are interesting in their own right.

1.2 GENOME EJECTION AND PACKAGING

Viruses depend on host organisms to reproduce. The life cycle of viruses generally consists of infection, genome replication and protein production, virion assembly, genome encapsidation, and exit from the host [10]. Although there are exceptions, this is true for many dsRNA and dsDNA phages. Outside the host, viruses exist as stable and inert virions. Since the lifecycle of eukaryotic viruses is complicated, this thesis focuses on viruses infecting bacteria and archaea. More specifically, the thesis focuses on genome ejection and packaging.

During infection, the genome of dsDNA bacteriophages is partly delivered by means of DNA ejection [11]. During infection the virus binds to the host and the genome is ejected into the cytosol. Ejection triggers have been isolated from certain host organisms. For example the LamB receptor protein triggers the ejection of bacteriophage λ [12]. Similarly membrane protein YueB triggers ejection from SPP1 [13]. The genome of the virus is tightly packaged into a small volume whose linear dimension is similar to the persistence length of the dsDNA. The genome settles into an ordered arrangement of co-centric loops [10]. Under such conditions, DNA is under significant pressure due to the elastic bending of the polymer and strong electrostatic repulsion caused by the negatively charged phosphate backbone. Energy stored as elastic bending and electrostatic repulsion drives the genome out of the capsid and partly into the host cytosol. Processes in the host then complete the internalization of the genome [14-16].

Infectious virus particles are assembled from components produced by the host during infection. Methods of assembly differ depending on virus type. In case of ssRNA phages the viral capsid co-assembles around the ssRNA genome, whereas in the case of dsDNA phages, the genome is actively packaged into a preformed capsid [17]. For certain dsRNA phages positive sense ssRNA fragments are packaged, after which in-capsid transcription completes the production of the dsRNA genome.

1.3 ARCHAEAL VIRUS HIS1

Archaeal viruses are the least studied viruses, with only 100 or so known species [18, 19]. Most known archaea and their viruses inhabit extreme environments, such as those with high salinity, temperature, pressure or acidity. Studying Archaeal viruses therefore furthers understanding of life under extreme conditions.

His1 is a spindle-shaped archaeal virus with a 14.464 kb linear dsDNA genome which infects an extremely halophilic archaeon *Haloarcula hispanica* [20, 21]. The His1 capsid [20], that is lemon shaped under certain conditions, is composed of one major and a few minor structural proteins. The major capsid protein features lipid modification [22]. Curiously, under high pH and

high temperature, the capsid transforms into an elongated tube, roughly equal in internal volume to that of the lemon capsid [23], paper I (Fig. 1). His1 has been found to eject its genome when subjected to high pH, high temperature, and to certain detergents (Fig. 1). Unlike certain bacteriophages, such as λ for which a triggering protein has been found [12], the natural trigger of His1 is unknown. One aim of this thesis work was to elucidate the ejection mechanism of His1 and then compare it to results obtained by studying bacteriophages (paper I). The starting point of the study was an osmotic suppression experiment. Cryo-EM studies have shown that His1 features a tightly packed dsDNA genome [23], much like many dsDNA bacteriophages. The similarity in this regard between His1 and certain bacteriophages prompted the study presented here. Numerous experiments on dsDNA bacteriophages have shown that DNA ejection can be modulated by the external osmotic pressure [10, 11, 24]. Osmotic pressure is induced by adding an inert molecule into the experiment buffer that cannot enter the capsid. This causes osmotic pressure across the capsid barrier which balances the force driving ejection. By varying external osmotic pressure by adding polyethylene glycol (PEG), the goal was to seek a point at which ejection is completely suppressed.

Archaeal organisms frequently habit extreme environments, such as those exhibiting high salinity and wide ranges of pH and temperature. Extending the DNA ejection experiments to include the effect of salinity and pH proved to be a natural continuation of the first part of the study. DNA ejection experiments were done in a range of mono- and divalent salt concentrations, pH, and temperatures. Salinity alters the electrostatic repulsion between the layers of packaged DNA through charge screening of the negatively charged backbone [6]. The motivation for the temperature study was supported by the recent finding of a phase change in packaged DNA observed in HSV-1 and λ [25, 26]. Under high pressure and above a certain temperature, DNA loses its regular packaging properties and becomes more fluid. This is thought to provide evolutionary advantage to such viruses in certain conditions, which can be explained by thermodynamics of the packaged dsDNA.

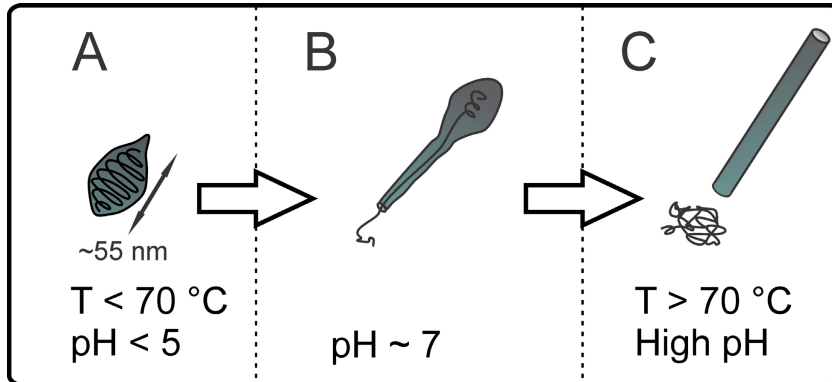


Figure 1 Schematic representation of His1 capsid transformation. (A) In low pH and temperature the lemon shaped capsid is filled with the dsDNA genome. The capsid elongates at increased temperature and pH (B, C). Ejection from the capsid is directional, with 5' end of the DNA being ejected first. For size of the capsid before and after transformation, see appendix A.

1.4 BACTERIOPHAGE PHI6

Most viruses causing serious disease in humans, animals, and plants have RNA genomes [27]. The focus of the genome packaging part of this thesis is on the dsRNA phage phi6, which features polymerase-level similarity with rotaviruses, a major cause of infant mortality [28].

Pseudomonas phage phi6 is a dsRNA phage member of the *Cystoviridae* family. It has a three part dsRNA genome inside a polyhedral virion (Fig. 2, S, M and L) [29]. However, only positive sense ssRNA segments (denoted by lower-case letters s^+ , m^+ , and l^+ , Fig. 2, C) are packaged and transcribed. Only ssRNA comes in contact with the cytosol of the host, thus protecting the dsRNA from a possible host response. The procapsid (or polymerase complex, PC) of phi6 is composed of coat protein P1, RNA-dependent RNA polymerase P2, packaging NTPase P4, and packaging factor P7 (Fig. 2, A). 120 copies of dimeric P1 compose the $T = 1$ icosahedral lattice common in dsRNA viruses [30]. The empty PC self-assembles in presence of these viral proteins, and is nucleated by P4 [31, 32] (Fig. 2, B). NTPase P4 is also responsible for packaging the ssRNA segments during virion assembly (Fig. 2, C). RNA segments are packaged in order from shortest to longest (s^+ , m^+ , l^+ , Fig. 2, C). In each case a specific *pac*-site at the 5' end of the genome binds to the procapsid, a step necessary before initiating the packaging [33-35]. Packaged ssRNA is transcribed into double-stranded genome fragments by P2 (Fig. 2, D). During infection, positive sense ssRNA segments are extruded from the procapsid (Fig. 2, E).

In solution ssRNA is strongly structured. During packaging, this structure needs to be opened by the helicase activity of P4. Additionally the volume of

the phi6 PC increases by 140-150% during the entire packaging/transcription process [36, 37]. Capsid expansion is needed to accommodate the whole genome, but the expansion also plays a role in selecting the packaged segment [37, 38]. After the s⁺-segment has been packaged, the capsid expands, reveals the binding site for the m⁺-segment *pac*-site, and hides the s⁺-segment site. Eventually the same thing happens for the l⁺-segment. This kind of orderly packaging is typical for dsRNA phages [39]. Whether this expansion is detectable by single molecule experiments is unknown. Packaging experiments with e.g. dsDNA phages like phi29 have resolved parameters such as the velocity, the stalling force of the packaging motor, and even the step size taken during packaging [40, 41]. Unlike dsDNA phages like e.g. phi29, dsRNA phages have not previously been subjected to single molecule OT experiments. Single molecule packaging experiments such as this may elucidate details of the packaging related to capsid expansion and opening of the ssRNA structure. Therefore, the goal of this study was to measure and characterize ssRNA packaging of phi6 and compare it with the results obtained from dsDNA phages.

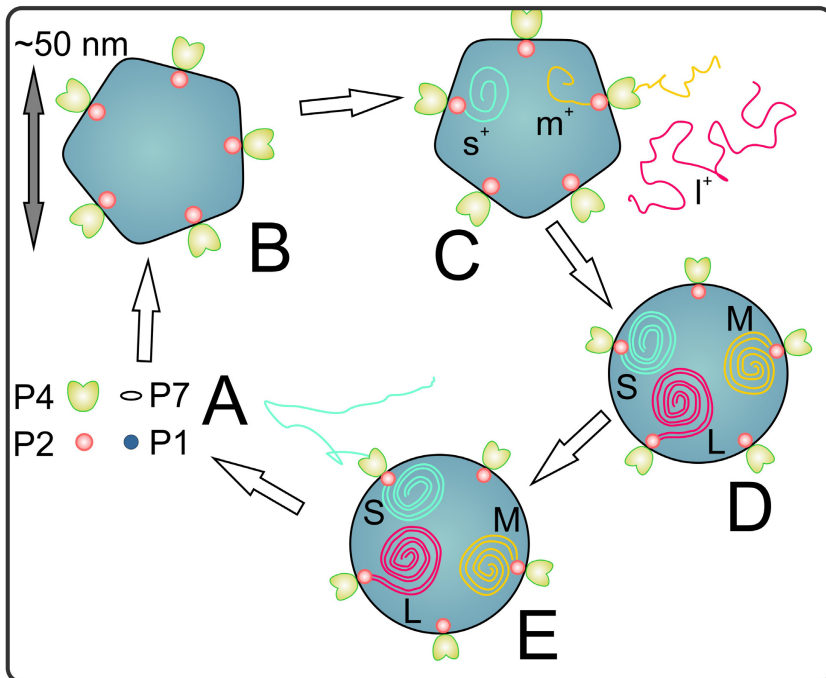


Figure 2 Schematic of Phi6 replication cycle. (A) Viral proteins assemble into an empty procapsid (B). Positive sense ssRNA fragments are packaged by P4. (D) Minus-sense ssRNA fragments are synthesized to produce the three-part dsRNA genome. (E) Positive sense ssRNA fragments are transcribed.

2 AIMS

The aim of this thesis work was to apply single molecule biophysics methods to the study of the viral lifecycle of archaeal virus His1 and dsRNA phage phi6.

Paper I investigated whether dsDNA ejection from His1 agrees with the prediction provided by continuum theory of packaging and ejection developed for bacteriophages. For this purpose, osmotic suppression experiments were designed. Since the host of His1 lives in high salinity environment, the effect of salinity on ejection was also of interest. DNA ejection was studied by TIRF microscopy *in vitro*. This was the first time single molecule experiments were performed on an Archaeal virus.

Paper II continued the dsDNA ejection work reported in paper I. Environmental effects of pH and temperature were studied in ranges relevant to the host of His1 and similar organisms. The predictions provided by the continuum theory regarding ejection force as a function of temperature were experimentally tested.

Paper III studied ssRNA packaging of phage phi6 using optical tweezers. Progression of packaging and packaging velocity were at the focus of the paper. Paper III provided the first report of an OT experiment on a dsRNA virus. For this purpose, a single molecule packaging assay was developed.

3 THEORY

3.1 CONTINUUM MODEL OF DNA EJECTION

DNA packaging and ejection of dsDNA phages can be mathematically modeled in different ways. Lately, two competing modeling methodologies have been established in the literature. Molecular dynamics simulations of simplified bead-on-strings models of DNA have successfully described the essential aspects of DNA packaging and ejection [42]. An alternative way employs a continuum model of the dsDNA packaged in a rotationally symmetric capsid [10]. A major difference between these two methods concerns the treatment of entropy. Details about this treatment are discussed in paper II and its references (especially [43, 44]). Friction effects are not considered theoretically due to mathematical intractability, and since the treatment considers free energy, it is assumed that the process is always close to equilibrium [10]. Nonetheless, the continuum model agrees well with osmotic suppression experiments conducted on bacteriophage λ . This model is relatively straightforward to use for theoretical analysis of DNA ejection [10].

The continuum model assumes that DNA is packaged as a stacked collection of concentric layers where each DNA loop forms a toroid with radius R' [10]. Schematic of packaged DNA in a His1 capsid is shown in Fig. 3. The cross-sectional arrangement of DNA in such packaging is hexagonal, which is supported by experimental evidence from packaged phage capsids [10, 45, 46]. The co-centric structure is well established by cryo-EM studies [17]. In a typical dsDNA phage, the DNA genome is packaged relatively tightly, so that the packaging ratio (volume of DNA divided by capsid volume) is 0.3-0.5 [10]. If DNA is packaged inside such a small volume two sources of resistance to packaging arise. First, packaging DNA in a radius close to the persistence length of dsDNA requires work against elastic repulsion. Secondly, the negatively charged phosphate backbone of DNA causes significant repulsion between the packaged DNA layers. Packaging in the continuum model is described by the free energy; the minimum energy needed to package a genome of length L into a capsid of a given shape and size.

The total free energy G_{tot} of the packaged dsDNA is given by:

$$(1) \quad G_{tot}(L, d_s) = \frac{2\pi\xi_p k_B T}{\sqrt{3}d_s} \int_R^{R_{out}} \frac{N(R')}{R'} dR' + \sqrt{3}F_0(c^2 + cd_s)L \exp\left(-\frac{d_s}{c}\right)$$

where R is the inner radius of the packaged DNA, R_{out} is the outer radius of the capsid, $N(R')$ is the number of DNA layers at position R' , d_s is the strand spacing in the hexagonal lattice, F_0 and c are semi-empirical parameters describing the effective strength of electrostatic repulsion [45], ξ_p is the

persistence length of dsDNA, k_B is the Boltzmann constant, and T is the absolute temperature. The first term in Eq. 1 represents the contribution from dsDNA bending, whereas the second term describes electrostatic repulsion.

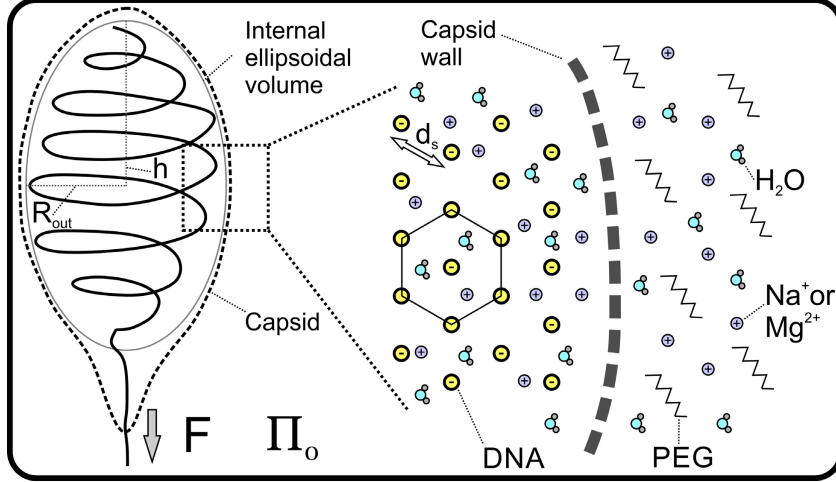


Figure 3 Schematic of DNA ejection from His1 with explanations of parameters and dimensions relevant to the continuum model. Right: Ellipsoidal internal volume highlighted in the His1 capsid. Left: Cross-section of the packaged DNA in hexagonal arrangement. Water and cations can permeate the capsid wall, while PEG cannot. R_{out} : Half-width of the ellipsoid, h : half-height of the ellipsoid, F : ejection force, Π_0 : external osmotic pressure. Molecule sizes and concentrations are not to scale.

The strand spacing d_s is obtained by minimizing the packaging free energy, which yields equation (2) [10]:

$$(2) \quad \sqrt{3}F_0 \exp(-d_s/c) = \frac{\xi_p k_B T}{R^2 d_s^2} - \frac{\xi_p k_B T}{d_s^2} \frac{\int_R^{R_{out}} \frac{z(R')}{R'} dR'}{\int_R^{R_{out}} R' z(R') dR'}$$

Here the integrals represent the dependence of free energy on capsid geometry, assuming rotational symmetry. The integral depends on the height of a DNA column $z(R') = N(R') \cdot d_s$, which characterizes the capsid shape. The His1 capsid can be modeled as an ellipsoid whose major axis is h and minor axis is R_{out} (Fig. 3). In this case the height of DNA column is (paper I):

$$(3) \quad z(R') = 2h \left(1 - \frac{R'^2}{R_{out}^2}\right)^{\frac{1}{2}}$$

Equation 2 can be numerically solved to yield d_s , the packaging force, and the osmotic pressure needed to suppress ejection. The packaging force F at a given length of packaged genome, L , is the derivative of the packaging energy with respect to packaged length [10]:

$$(4) \quad F(d_s(L), L) = \sqrt{3}F_0(c^2 + cd_s) \exp(-d_s/c) + \frac{\xi_p k_B T}{2R^2}$$

Maximum packaging force is given by Equation 4, when the entire genome is packaged. Maximum packaging force affects the ejection velocity. Predicting the functional form of the velocity during ejection would require knowledge of the various sources of friction in the system. Since this is impractical, the effect of the resisting force can be estimated as follows. Assuming that ejected DNA forms a spherical globule of radius $r_{globule}$, the drag force experienced by the globule is given by Stoke's law:

$$(5) \quad F_v = 6\pi\eta r_{globule} v$$

where η is the dynamic viscosity of the liquid medium and v is the velocity of the globule. Hence increasing the driving force increases the velocity. The osmotic pressure Π_0 needed to suppress an ejection of length L is:

$$(6) \quad \Pi_0 = \frac{F(d_s(L), L)}{\pi R_{DNA}^2},$$

where R_{DNA} is the effective radius of the end of the dsDNA strand, and where the packaging force and strand spacing depend on the amount of packaged DNA. Equation 6 essentially describes the balance between the force and pressure-volume-work required to move DNA into the surrounding liquid with a specified osmotic pressure. The effect of the presence of an osmolyte, e.g. PEG, can be described using Eq. 6, and is due to the fact that PEG cannot permeate the capsid wall (Fig. 3). On the other hand, mono- or divalent cations can enter the capsid and directly reduce electrostatic repulsion due to charge screening. The semi-empirical parameters F_0 and c describe this effect and are specific to particular salinity conditions.

Further, by taking into account the temperature dependence of the persistence length of dsDNA, one can calculate these packaging parameters as a function of temperature. The second term in Eq. 4 increases slightly with temperature. This effect is counteracted by a decrease in persistence length with temperature [47]. The net effect is that the maximum packaging force increases weakly with temperature (Fig. 17 and II).

4 METHODS

4.1 OPTICAL TWEEZERS WITH FLUORESCENCE MICROSCOPY

Figure 4 shows an optical tweezers (OT) instrument with total internal reflection fluorescence (TIRF) capability. The OT part of the instrument has been described in detail earlier [6-8, 48, 49]. The instrument is built around a commercial inverted microscope (Nikon TE-2000), which provides camera ports and focusing mechanics. An Nd:YAG laser operating at 1064 nm is used for optical trapping (Coherent Compass 1064-4000). The OT is based on dual-beam configuration with one beam steerable in the image plane by an acousto-optic deflector (AOD, NEOS Technologies 45035-3-6.5DEG-1.06-XY). The back-focal plane of the objective (Nikon CFI Apo TIRF 100X, NA = 1.49, oil immersion) is imaged using a 1X Keplerian telescopes into the AOD, which facilitates beam steering. Separate diode lasers (Hitachi HL7851G, 785 nm and Thorlabs DL5032-001, 830 nm) are used for position detection in a back-focal-plane configuration. Position signals measured by position sensitive detectors (PSD, SiTek S2-0171) are digitized using a DAQ-board with an integrated FPGA (National Instruments PCI-7833R). Proportional-integral-derivative (PID) feedback is implemented in the FPGA to allow fast (200 kHz) position and force clamping. Constant force feedback was achieved in the experiments of paper III with an integrative controller (non-dimensional gain constant of 2⁻⁴). LabVIEW-based control software is used to operate the instrument. A standard CCD camera (Panasonic WV-BP100/G) is used for visual guiding during the experiment.

TIRF-capability was implemented on the same optical axis where the optical trap works. A diode-pumped semiconductor laser operating at 488 nm (Coherent Sapphire 488-50) is used for fluorescence excitation. The polarization direction of the laser beam can be adjusted by a half-wave plate placed adjacent to the laser aperture (Fig. 4, ThorlabsWPH05M-488). The output beam from the laser is expanded 30× with Galilean telescopes (Appendix A), after which the expanded beam is guided to the optical axis of the system by a dichroic mirror (D1, Fig. 4, Semrock 495-Dio3). A plano-convex lens (L5 in Fig. 4, Thorlabs LA-1725-A, f = 400 mm) is placed before the dichroic mirror to focus the light onto the back-focal plane of the objective. This provides wide-beam excitation at the surface of the cover slip. The focusing lens L5 can be laterally translated using a micrometer stage to switch between the epifluorescence and TIRF geometries. By displacing L5 sufficiently so that the incident beam angle exceeds the critical angle, the excitation beam is totally internally reflected from the coverslip-water interface. This results in exponentially decaying localized excitation which greatly suppresses background emission from the channel, Fig. 4, C. Emitted

fluorescence light passes the objective and dichroic mirror and is band-pass filtered (F1 in Fig. 4, Semrock 520/35-23) before it is imaged by an electron multiplying CCD (EMCCD) camera (Andor iXon, DU-897). The control software for fluorescence imaging and acquisition is implemented in LabVIEW 2011 (National Instruments). The immersion oil used in the experiments (Leica type N, $n = 1.518$ at 546 nm) gave no significant background fluorescence.

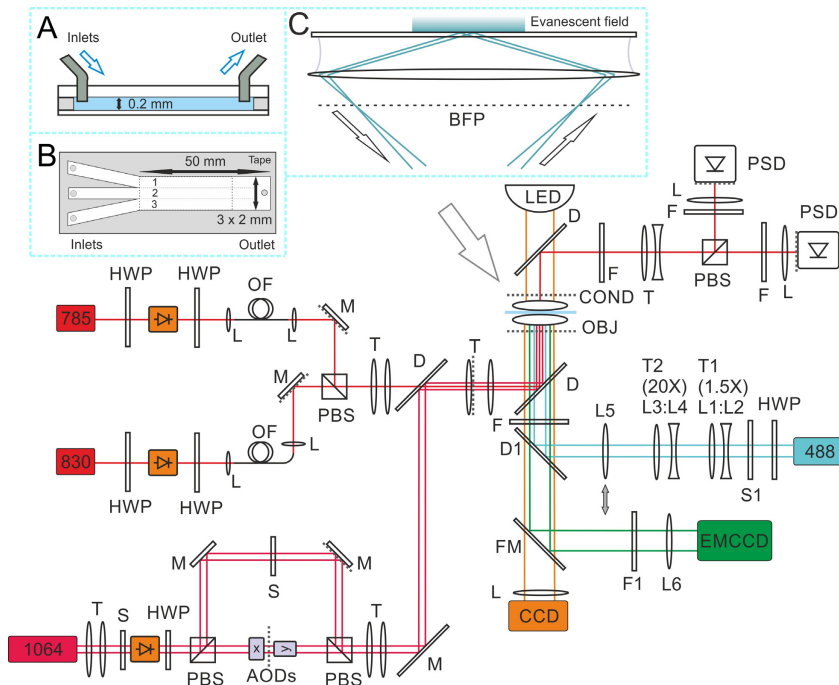


Figure 4 Schematic of the combined optical tweezers and TIRF microscope. Unnumbered parts correspond to optics described earlier in [8]. Numbered parts comprise the TIRF part of the instrument. Inset: (A) Side view of the flow cell. (B) Three-channel flow cell used in the optical trapping experiments. (C) Total internal reflection geometry used in fluorescence experiments. Abbreviations: T: telescope, L: lens, HWP: half-wave plate, PBS: polarizing beam splitter, AOD: acousto-optic deflector, M: mirror, D: dichroic mirror, OF: optical fiber, FM: flip mirror, PSD: position sensitive detector, S: shutter, F: optical filter, OBJ: microscope objective, COND: condenser lens, LED: light emitting diode. BFP: back focal plane. Dashed lines indicate locations of optically conjugate planes. Boxed number indicates a laser with respective wavelength in nanometers. For list of components see appendix B.

4.2 ASSAY PREPARATION

4.2.1 HIS1 EJECTION ASSAY

The growth and purification of His1 particles are described in detail in [22].

The ejection buffer was based on Tris-buffer (50 mM NaCl, 3.5 mM MgCl₂, 10 mM KCl, 1 mM CaCl₂, and 50 mM Tris-HCl) with pH 7.2 in control experiments. SyBR Gold dye (Nucleic acid stain, Invitrogen, cat. no. S11494, diluted 5×10^{-6} , fluorescence emission centered at 537 nm) was used for fluorescent detection. Concentrations of NaCl, MgCl₂ and polyethylene glycol 300 (PEG300, Sigma-Aldrich) were changed accordingly to match the desired conditions in osmotic suppression experiments. The PEG300 concentration was chosen to set the osmotic pressure according to the model described in [50]. For pH dependent experiments, Tris or Bis-tris buffer with the required pH value was used. Temperature-dependent experiments were carried out in standard Tris-buffer (pH 7.2).

His1 DNA ejection experiments were conducted in a single-channel flow chamber constructed by attaching a cover slip ($60 \times 24 \times 0.17 \text{ mm}^3$) to a microscope glass ($75 \times 25 \times 1 \text{ mm}^3$) using double-sided tape (Tesa AB, thickness 0.2 mm). The channel shape was cut into the tape, and fluid inlet/outlet holes were drilled into the microscope glass. PEEK tubing (Supelco Inc., 0.25 mm inner diameter) was glued with UV-curable epoxy (Norland products NOA81) to provide inlets and outlets for the fluid flow.

The chamber was prepared by etching the cover slip in a detergent solution (0.5%, Alconox) at 95°C for 1 h. Next, the cover slip was rinsed in purified water and dried in filtered and pressurized air. Immediately afterwards the cover slip was attached to the tape and sample containing His1 capsids was injected into the chamber. The injected sample was left in the chamber for 15 min in room temperature (RT) in order for the capsids to bind nonspecifically to the etched glass surface.

The experiment was initiated by injecting ejection buffer with 0.05% Triton X-100 (Sigma Aldrich) with a microfluidic injector. A constant flow of 100 μl / min was applied with a syringe pump (Harvard Apparatus) to stretch the ejected DNAs. After the ejection in the field of view was complete (no more new ejection events were observed), the chamber was translated using a piezo-motor stage (Physik Instrumente M-686.D64) to a new position in the channel. The image was refocused and recorded. This procedure was repeated to get ejection statistics data. This full frame data (512×512 pixels, exposure time 30 ms, EM gain 180) were collected at 15 fps.

Single event measurements used for velocity calculations were performed similarly. The image was refocused to a spot on the glass surface with unejected His1 capsids visible in the fluorescence image. Buffer containing Triton was injected, and the progression of the ejection was recorded. This was repeated to get statistics on the events. For single event experiments, the frame

size was reduced by half (256×256 pixels, exposure time 15 ms, EM gain 200) in order to increase frame rate to 58 fps.

Temperature in the flow cell was controlled by a custom built aluminum heating block mounted on the objective. Water heated by a heat bath (MGW Lauda MT) was circulated through the block to set the temperature of the sample chamber. Temperatures below room temperature were achieved by circulating and heating water from an ice bath.

4.2.2 PHI6 PACKAGING ASSAY

The preparation of phi6 procapsids is described in paper III.

All experiments took place in packaging buffer (50mM Tris (pH 8.9), 2 mM dithiothreitol (DTT), 0.1 mM EDTA, 2.5 mM $MgCl_2$, 6% polyethylene glycol (PEG) 4000, 6000 or 20000, and 80 mM NH_4Ac [51, 52]).

Phi6 packaging experiments were conducted in a three-channel flow chamber assembled similarly as described in the previous section. The channel dimensions were $6 \times 50 \times 0.20$ mm³. A schematic of the three-channel chamber in shown in the inset in Fig. 4, A. Laminar flow created by the syringe pump kept the contents of the channels from mixing with each other. Prior to use, the chamber was blocked/passivated with TEW-buffer containing 5 mg / ml BSA for 30 min in RT, after which the chamber was flushed by injecting 1 ml of TE buffer.

The first channel of the flow cell contained biotinylated s⁺-segment or sml⁺ ssRNA bound to streptavidin-coated polystyrene beads from the 3' end (1.87 μ m diameter, Kisker Biotech). The second channel carried protein-G-coated polystyrene beads (2.1 μ m diameter, Kisker Biotech) with antibody bound procapsids (1K1 [53] against coat protein P1, or 4S8 against packaging NTPase P4 [54]), while the third channel carried packaging buffer with or without ATP (0 or 1 - 10 mM, paper III).

The experiment was initiated by trapping a SA-coated bead in the first channel, the trapped bead was moved with the piezo-stage to the second channel where a PG-coated bead was trapped. The two beads were moved next to each other in order to bind the 5' end of the s⁺-segment ssRNA to the procapsid. This formed an ssRNA tether between the beads. A schematic of the double-trapped assay is shown in Fig. 5. When a tether formed, the dumbbell was moved into the third channel, where it was clamped to a constant force and the experiment was initiated. The experiment continued for 20 minutes or until the tether broke spontaneously.

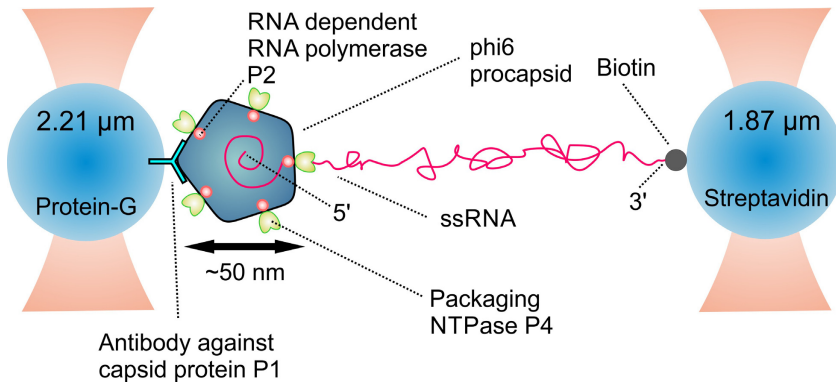


Figure 5 Schematic of the phi6 packaging assay (not to scale).

4.3 DATA ANALYSIS

4.3.1 FLUORESCENCE IMAGES

The fluorescence images of the His1 ejection experiments were analyzed semi-automatically with a custom-designed data analysis procedure (papers I, II). The data analysis is schematically depicted in Fig. 6. The raw data is in the form of a video of ejected or ejecting DNA molecules illuminated by the TIRF excitation at the coverslip surface. Well-focused video frames featuring ejected DNAs were manually selected. Each selected frame was subjected to an automatic image segmentation algorithm that counted the ejected DNA molecules in the frame and calculated their lengths. All data analysis steps were done in MATLAB.

The algorithm starts by low-pass filtering the frame with a Gaussian-kernel image filter (3×3 pixels, $\sigma = 1.5$), which is followed by Canny edge detection [55] (threshold parameters: low: 0.01, high: 0.2), that identifies the peripheries of the individual DNA molecules. These molecules were subsequently located and counted using MATLAB's *bwconncomp*-function. The length of the individual DNA molecules was calculated as the Euclidean distance between the left and right edges of the edge-detected frame (Fig. 6, D).

The uncertainty of the length calculation was estimated using the law of error propagation. When assuming that the uncertainty in locating both ends of the DNA is equal to the pixel size in the image, the uncertainty in length is $\sqrt{2} \cdot dx$, where dx is the pixel size. In the experiments concerning the ejection statistics the pixel size was 106.7 nm, which yields an uncertainty of 150.9 nm.

From these data the average number of ejected DNAs per field of view and the corresponding length histograms were calculated. The uncertainties

represented by error bars in the respective plots are sample standard deviations of the respective values.

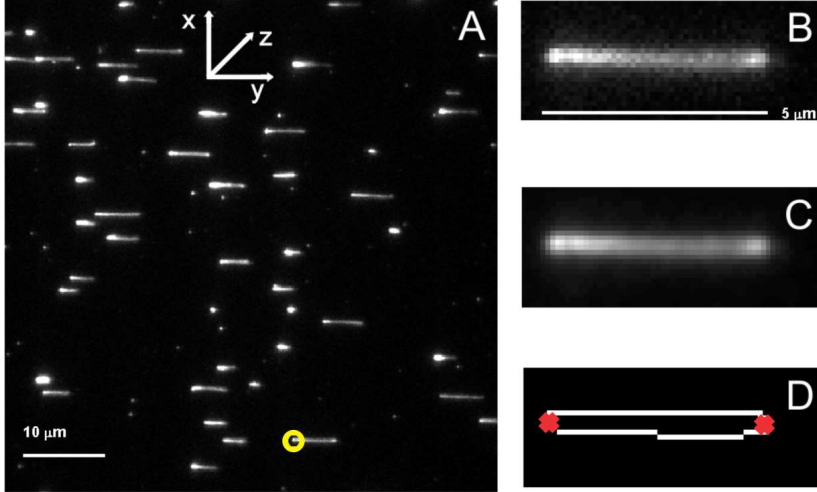


Figure 6 Schematic of data analysis procedure in the fluorescence microscopy experiments. (A) Fluorescence image recorded in a control experiment, with a selected DNA marked with a circle. (B) Magnified image of the selected DNA. (C) Low-pass filtered image of the selected DNA. (D) Edge detected image of the DNA, with marked positions of the left and right ends.

The data analysis in the ejection velocity measurements was similar to the case of the ejection statistics data. Ejecting DNA molecules were identified manually from the video. For each point in time during the ejection, the length of the ejected DNA molecule was automatically calculated as described above. This procedure gave the ejected length as a function of time. The ejection velocity was calculated using standard five-point differentiation [56]. The maximum ejection velocity was calculated for each molecule to represent the speed of ejection.

4.3.2 OPTICAL TWEEZERS MEASUREMENTS

4.3.2.1 Calibration

For optical trapping measurements in paper III, data analysis was carried out essentially as described previously [6-8, 48, 49]. The trapped particle is subject to a 3D harmonic potential, described at small displacements by a stiffness constant k_j , where $j \in [x, y, z]$ is the spatial coordinate, with the trapping beam propagating in the z -direction. Position detection calibration

was done in multiple steps. Pixel size of the video frame was calibrated using a micromachined size standard (Graticules Inc., $50 \times 2 \mu\text{m}$, CS2370), which gave the size of an image pixel ($\mu\text{m} / \text{px}$). AOD movement was calibrated by displacing a trapped bead in a rectangular grid, and comparing the result to apparent size in the video image. This gave the sensitivity of the AOD ($\mu\text{m} / \text{MHz}$). Finally, a trapped bead was moved with the AOD in a rectangular grid in the image plane (x,y -plane) over the linear detection region of the detector spot. A linear 2D function was fitted to the resulting detector response to get the position sensitivity of the trap (in $\mu\text{m} / \text{V}$).

Stiffness calibration of the trap was done by fitting a Lorentzian function to the power spectral density of bead displacement. The one-sided 1D power spectral density of the movement of a trapped bead subject to Brownian motion of the surrounding liquid is given by a Lorentzian function [4]:

$$(7) \quad S_j = \frac{k_B T}{\pi^2 \beta (f^2 + f_c^2)},$$

where $\beta = 6\pi\eta a$ is the drag coefficient, η is the dynamic viscosity of the buffer, and a is the bead radius. The corner frequency f_c is:

$$(8) \quad f_c = \frac{k_j}{2\pi\beta}.$$

The motion of a trapped bead was recorded for 10 s, from which PSD was calculated using MATLAB's implementation of Welch's spectral estimation algorithm. Three PSDs from three consecutive 10 s-measurements were averaged, to which a Lorentzian function (Eq. 6) was fitted to get f_c , which in turn yielded the trap stiffness k_j (in pN / μm).

4.3.2.2 Packaging velocity

Packaging experiments were carried out in a two-trap configuration, Fig. 5. The apparent length of the packaged RNA is:

$$(9) \quad x(t) = L_{RNA, fold}(t) + v_{P4}(t)t + d_{capsid}(t),$$

where $L_{RNA, fold}$ is the length of the folded ssRNA, v_{P4} is the instantaneous packaging velocity of P4, and $d_{capsid}(t)$ is the time-dependent expansion of the PC. When no opening of secondary structures occurs and assuming that the expansion of the procapsid is negligible, the apparent shortening of the tether corresponds to the packaging action of P4.

Assuming that the aforementioned conditions hold, the instantaneous packaging velocity is given by direct numerical differentiation of the packaged length. A standard five-point method was used for this purpose [56]. The employed sign notation makes net packaging have negative velocity values. Positive velocity indicates increase in length caused by e.g. opening of secondary structures or by procapsid expansion.

Prior to numerical differentiation the packaged length data was low-pass filtered with a zero-phase 12th order Butterworth filter with a corner frequency of 0.1 Hz.

The mean packaging velocity was calculated from the histogram of filtered velocity values using a Gaussian fit to the histogram. The spread in velocity values is described by the spread parameter (cf. standard deviation) of the fit.

4.3.2.3 Packaging in sections

The packaged length data was analyzed to discriminate between fast and slow packaging sections for the purpose of visualization. Low-pass filtered length data was windowed into 3 s long sections, in which the average packaging velocity was calculated as described above. If the average packaging velocity was below -0.4 nm / s, the section was deemed “fast”, otherwise the section was considered to be “slow”.

A region of interest (ROI) in each successful packaging experiment was chosen to further analyze the first ~100 nm of packaged ssRNA. This 100 nm corresponds roughly to the *pac*-site at the beginning of the *s*⁺-segment. The amount of packaged RNA in each section was calculated for the ROI.

5 RESULTS

5.1.1 DNA EJECTION FROM HIS1

Representative single ejection traces in standard buffer conditions (Tris, pH 7.2, 50 mM NaCl) are shown in Fig. 7, A. The average maximum ejection velocity was $48.97 \pm 24.48 \mu\text{m} / \text{s}$ ($144 \pm 72 \text{ kbp} / \text{s}$). Single DNA traces show random pauses 0-2 times during ejection. Ejection time (10% - 90% rise time) had a median value of 190 ms, with certain ejections taking up to 1.2 s. A fluorescence image of ejected DNA after injection of Triton X-100 is shown in Fig. 7, C. The ejection is on average incomplete, which is shown by the length histogram of the control experiment (Fig. 8, C). The average ejected lengths range from very short to essentially full genome length, with a maximum at 5 micrometers.

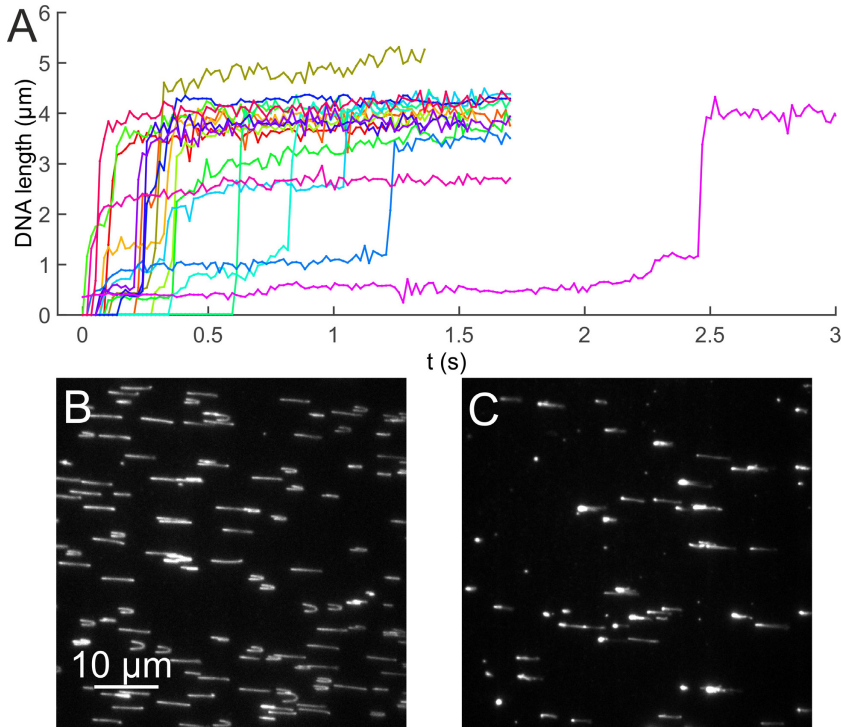


Figure 7 (A) Single ejection traces of His1 ejection in Tris buffer (pH 7.2). (B) TIRF image of plain His1 DNA molecules on etched glass. (C) TIRF image of DNA ejection in Tris buffer (pH 7.2).

5.1.1.1 Directionality of ejection

To investigate whether DNA ejection is directional (same end always exits first), a restriction enzyme experiment was conducted. The His1 genome has two sites suitable for the restriction enzyme DraI [20], dividing the genome into three parts (schematic in Fig. 8, top). Figure 7, B shows plain His1 dsDNA molecules attached nonspecifically to the cover glass surface by the terminal proteins at the ends of the molecule. The length histogram of the plain DNAs is shown in Fig. 8, A. The apparent length of the plain DNAs ($5.28 \pm 0.13 \mu\text{m}$) is longer than what is expected from the genome length (14.464 kbp, or $4.918 \mu\text{m}$), which is due to lengthening caused by the intercalating SyBR Gold dye. Intercalating dyes have been observed to increase the contour length of dsDNA by a factor 1.1-1.2, which agrees with our observations [57]. Subjecting plain DNA molecules to a restriction enzyme (see methods in paper I) results in two length groups of DNA fragments (Fig. 8, B), corresponding to fragments II+III and I. The middle fragment does not attach to the glass, and therefore is not visible. Repeating the restriction enzyme experiment with ejected DNA from His1 capsids creates a length histogram centered at $\sim 1 \mu\text{m}$ (Fig. 8, D), where the lengths of the ejected DNAs are significantly shorter than in the case of ejection from an untreated sample (Fig. 8, C). The His1 capsid protects the unejected part of the genome from digestion. The result in Fig. 8, D suggests that the I-fragment was cleaved off, leaving the segment II+III attached to the capsid. Therefore, DNA ejection with fragment I (5' end) first.

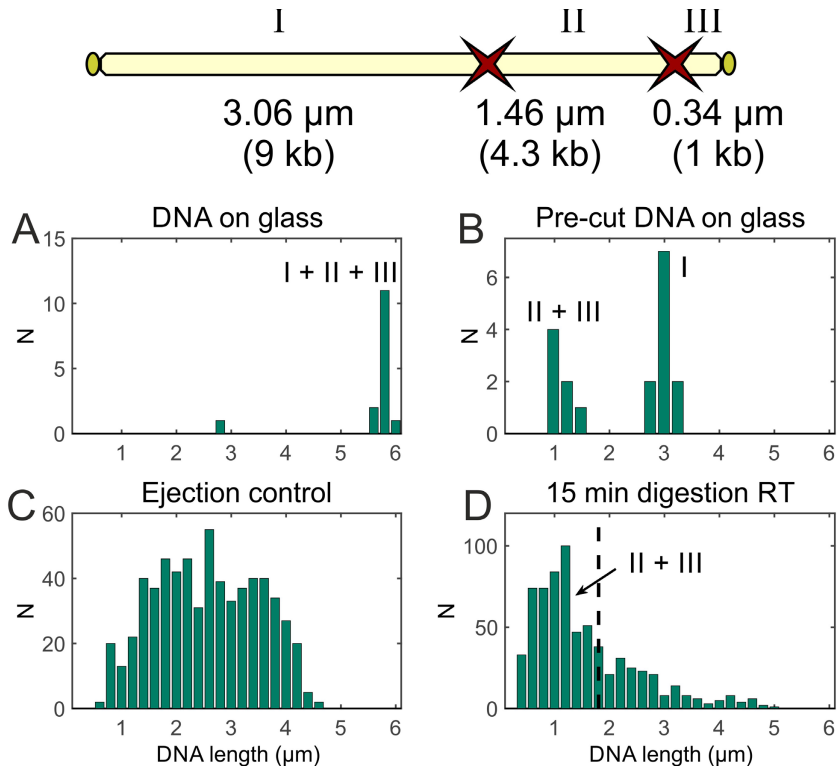


Figure 8 Ejection directionality from His1. Top part of the image shows restriction enzyme sites, which divide the genome into three parts. Ellipses at the end of the DNA are the terminal proteins which bind nonspecifically to the glass surface. (A) Lengths of plain undigested DNAs on glass. (B) Digested DNAs on glass with end products divided into two separate peaks in the histogram. (C) Length histogram of ejected DNAs in Tris-buffer. (D) Length histogram of ejected DNAs subjected to 15 min of digestion by the restriction enzyme. End product II+III is primarily left intact. Black dashed line corresponds to the 5.3 kb-long II+III fragment.

5.1.1.2 Osmotic suppression experiments

Results of an osmotic suppression experiment, where the osmotic pressure was varied by adding PEG300 to the experiment buffer, are shown in Fig. 9, A. The number of ejected DNAs drops with increasing PEG300 concentration nearly monotonically and then practically vanishes at 10% (9.9 atm). In the length histogram view this is evident as a gradual reduction in the average length of the ejected DNA molecules (Fig. 10). Below 10% PEG300 the shape of the histogram changes only slightly (Fig. 10, A-D). Whereas at higher concentrations the fraction of short DNA molecules increases abruptly (Fig. 10, E-F). This behavior corresponds qualitatively to the prediction by the

continuum theory (Fig. 11, C), although the theoretical model is quite sensitive to any change in capsid size, as indicated by the confidence limits in Fig. 11. The simulated strand spacing is 2.6 nm for the fully packaged ellipsoidal capsid (Fig. 11, A). A similar value has been observed in the case of many bacteriophages. The maximum simulated packaging force is 15 pN (Fig. 11, B).

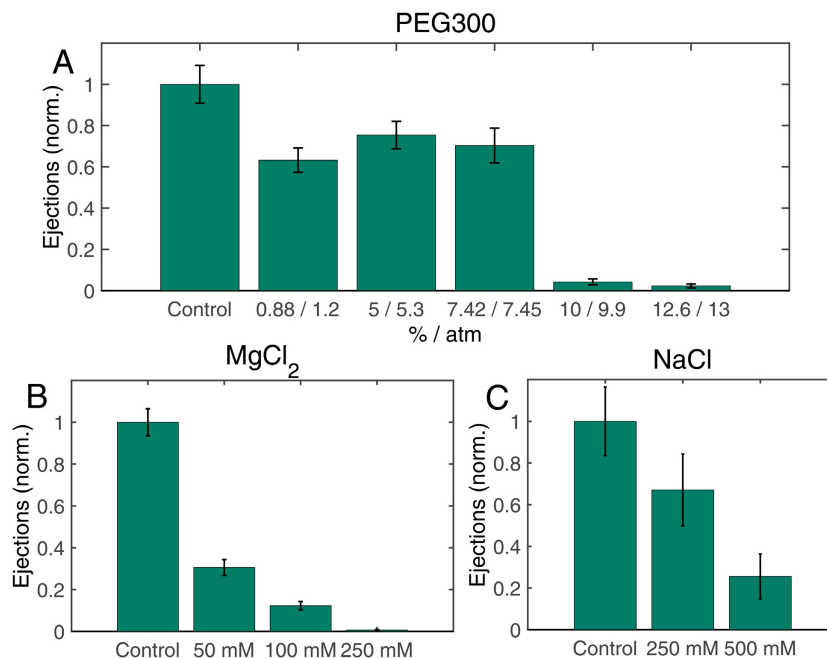


Figure 9 Normalized number of ejection events (A) as a function of PEG300 concentration, (B) MgCl₂, and (C) NaCl. The number of ejection events was normalized to that of the control sample. Error bars represent one sample standard deviation in each experiment.

5.1.1.3 Effect of salts

The effect of mono- and divalent salts was investigated by adding NaCl or MgCl₂ to the ejection buffer. Results for the number of ejected DNA molecules in NaCl and MgCl₂ experiments are shown in Fig 9, B and C, respectively. The number of ejected DNAs decreases with increasing NaCl concentration in a roughly linear manner. On the other hand, the effect of Mg²⁺ ions is more pronounced. MgCl₂ concentration of 50 mM is required to reduce the number of ejections to approximately one-fifth of the value in the control experiment (Fig. 9, B). A much larger concentration of 500 mM of NaCl results in a similar reduction of ejections (Fig. 9, C). A similar effect is shown in the length histogram data (Figs. 12 and 13). Even a minor increase in Mg²⁺ concentration (50 mM, Fig. 12, B) results in presence of only short DNAs (Fig. 12, B-D).

Results

Change in NaCl concentration causes a more gradual change in ejected lengths. Even at 500 mM of NaCl (Fig. 13, C), the shape of the histogram changes only slightly, although the number of ejected DNAs diminishes.

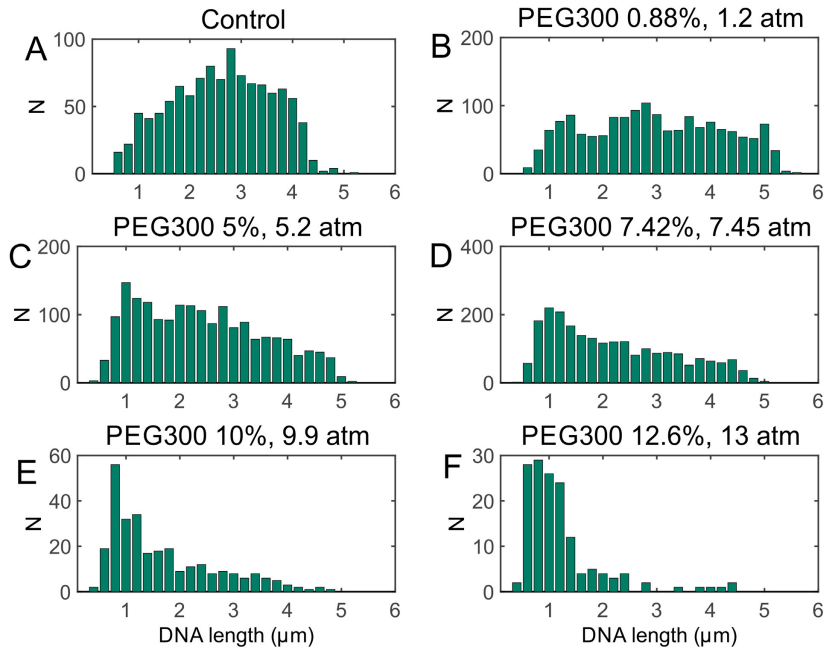


Figure 10 Length histograms of DNA ejected DNA from His1 with increasing PEG300-induced osmotic pressure.

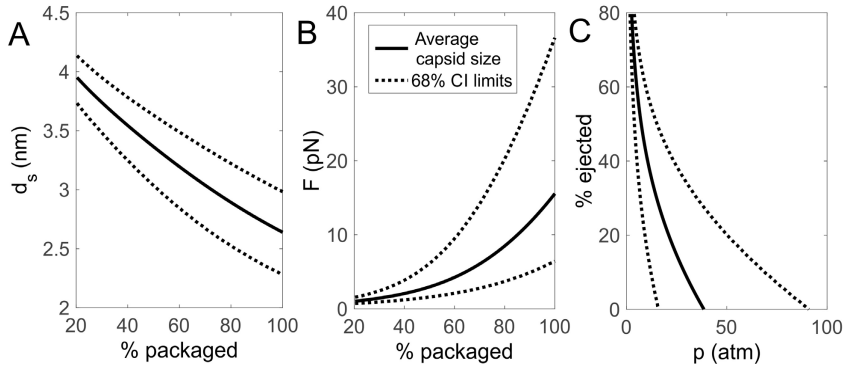


Figure 11 Predicted packaging and ejection properties of the His1 capsid according to the continuum theory, with capsid dimensions specified in paper I. (A) DNA strand spacing as a function of % of genome packaged. (B) Packaging force as a function of % of genome packaged. (C) Osmotic pressure needed to suppress ejection. Dashed line curves correspond to 1-sigma confidence intervals (68%), when the capsid dimensions were varied 10%.

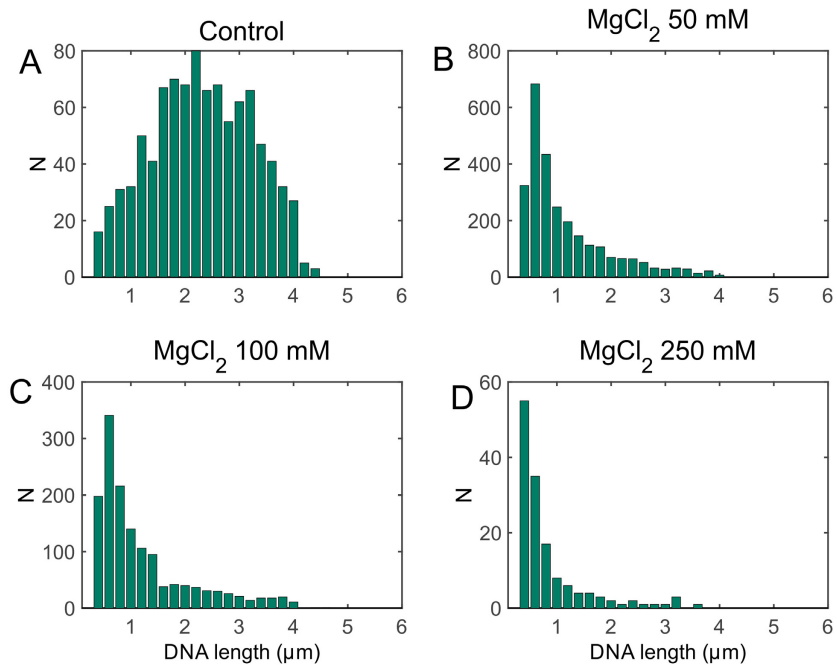


Figure 12 Length histograms of ejected DNA from His1 with increasing MgCl_2 concentration.

Results

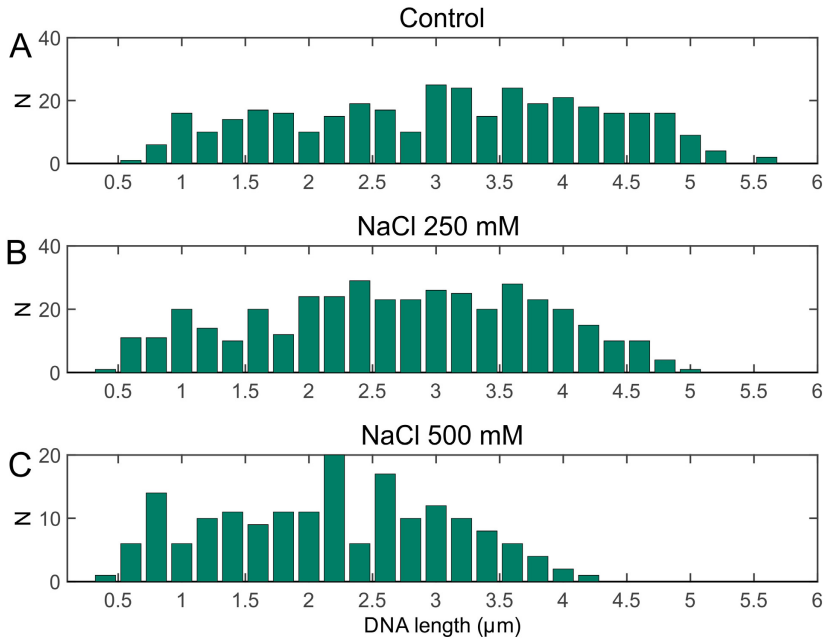


Figure 13 Length histograms of ejected DNA from His1 with increasing NaCl concentration.

5.1.1.4 Effect of pH

The effect of pH on DNA ejection was investigated in a range of pH values (pH 4.5 - 9). Figure 14 shows the number of ejections per field of view as a function of pH. For slightly acidic pH (> 4.5) the number of ejections was essentially stable, while an increase was observed for pH > 7.2. Below pH 4.5 ejections were essentially suppressed with no ejected DNA visible (data not shown).

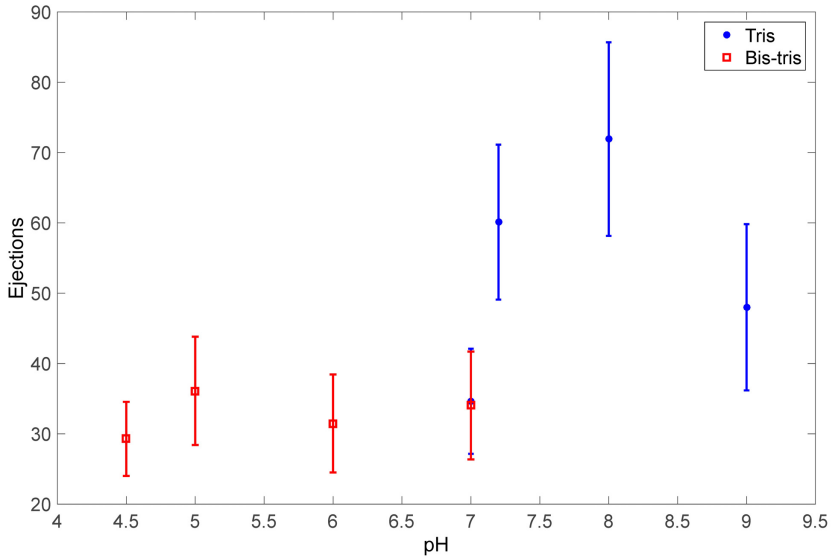


Figure 14 Number of ejections as a function of pH. All data points correspond to N = 37 frames.

5.1.1.5 Effect of temperature

The effect of temperature to ejection was investigated within 15 - 42°C. The number of ejections as a function of temperature is shown in Fig. 15. Maximum efficiency is observed around 32°C, with the number of ejections diminishing at both high and low temperatures.

The maximum ejection velocity exhibits considerable variation, but has a statistically significant positive slope ($0.89 \pm 0.41 \mu\text{m} / \text{s} / ^\circ\text{C}$, F-statistic: 18.51, $p < 0.0001$, N = 336) as a function of temperature (Fig. 16). This can be compared to the theoretically predicted maximum packaging force as a function of temperature for four classes of capsid size (Fig. 17). Regardless of capsid size, the maximum packaging force increases weakly with temperature. Graphs in Fig. 17 correspond to four classes of capsid size observed among His1 [23]. Capsid sizes are tabulated in Appendix A.

Results

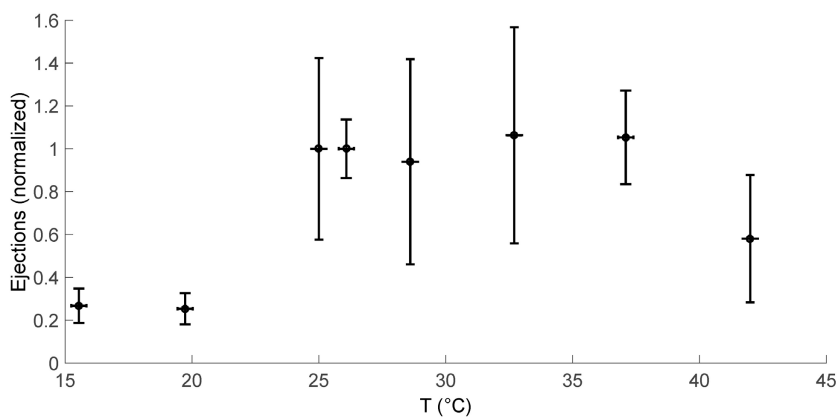


Figure 15 Normalized number of ejections as a function of temperature. Error bars represent sample standard deviation at each temperature. Number of ejections is normalized to the average value measured at 25°C (N = 37).

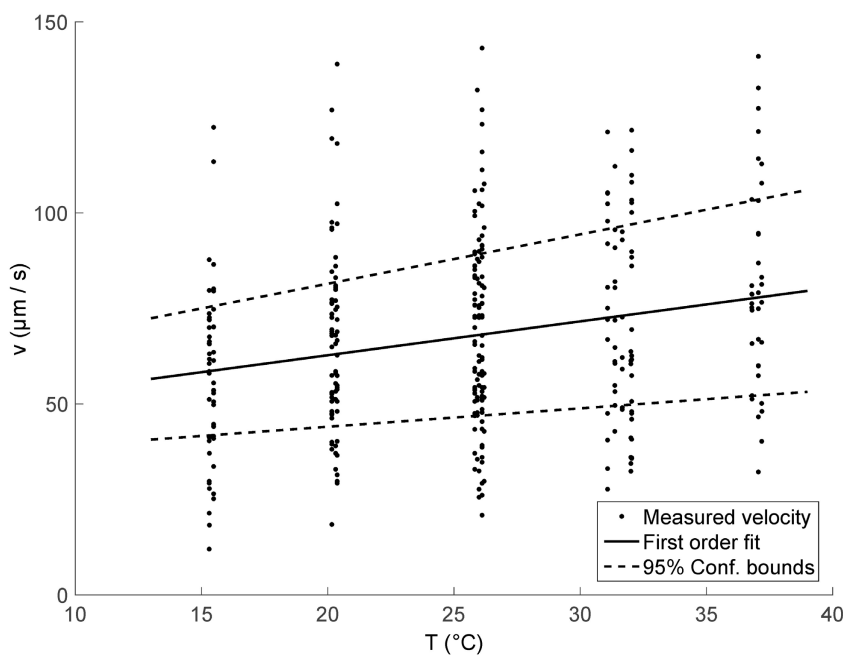


Figure 16 Maximum velocity during DNA ejection as a function of temperature. First order fit has a statistically significant slope of $0.89 \pm 41 \mu\text{m} / \text{s} / ^\circ\text{C}$ (F-statistic 18.51, $p < 0.0001$, N = 336).

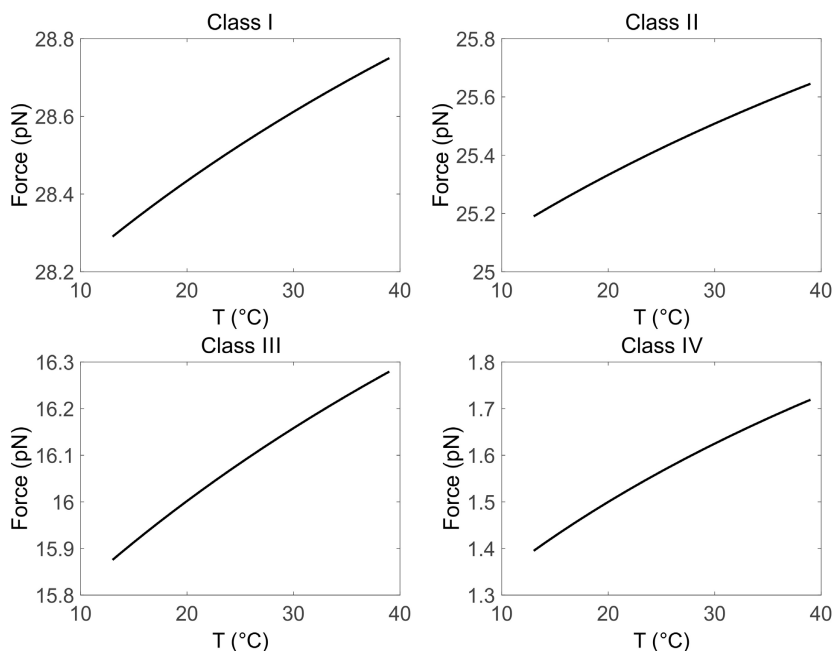


Figure 17 Theoretically predicted maximum packaging force at full packaging for four capsid size classes of His1 (Appendix A) as a function of temperature.

5.1.2 SINGLE-STRANDED RNA PACKAGING OF PHI6

5.1.2.1 Average packaging velocity

In vitro ssRNA packaging experiments were carried with OT using constant force feedback. Out of 445 positive OT experiments in the presence of ATP, 24 showed packaging action, which gives an efficiency of 5.4%. A representative packaging trace of phi6 is shown in Fig. 18 A, while a comparable graph from a control experiment measured in the absence of ATP is shown in Fig. 18, B. Corresponding histograms of instantaneous packaging velocities are shown in Fig. 19. The average packaging velocity for the positive experiment was -0.32 ± 0.62 nm / s (-0.94 ± 1.83 nt / s). The mean value for all positive experiments was 0.07 - 0.54 nm / s (paper III, supplementary data). The corresponding value for the control experiment was -0.03 ± 0.58 nm / s, due to instrument drift. The mean value for all control experiments was -0.048 ± 0.055 nm / s.

Results

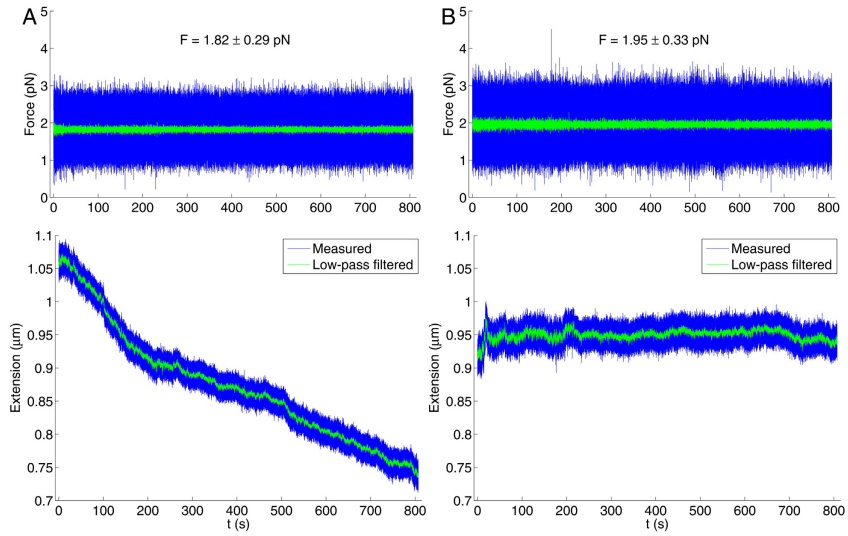


Figure 18 Representative tether length traces of phi6 packaging experiments. (A) with 10 mM ATP in the packaging buffer. (B) control experiment without ATP. Top panels show the force acting of the tether, which is maintained at a constant value with feedback.

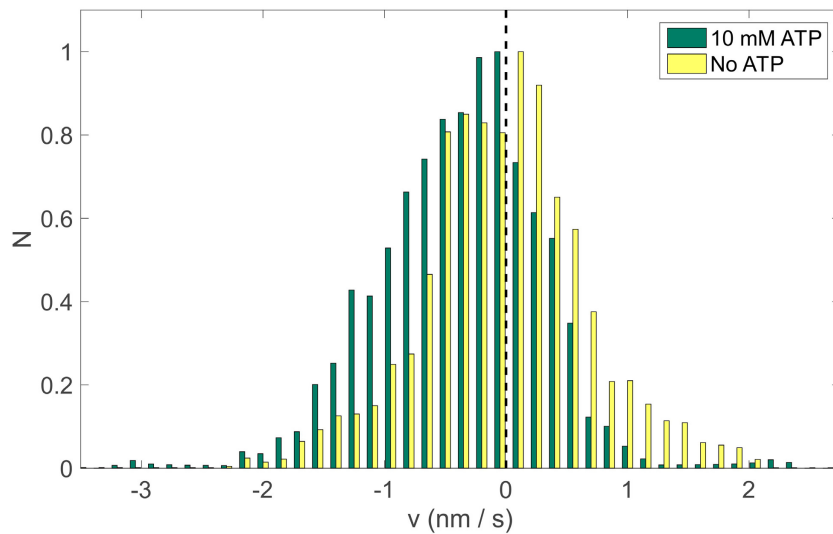


Figure 19 Velocity histograms of phi6 packaging experiments of Fig. 18 with and without ATP. Histograms are normalized to the maximum value for both data sets. Black dashed line indicates zero velocity.

5.1.2.2 Packaging alternates between fast and slow sections

Low-pass-filtered and velocity discriminated traces of eight successful positive experiments are shown in Fig. 20. Markers and color coding, as defined in methods, indicate ROIs in Fig. 20. All traces show alternating fast and slow packaging sections. Similar behavior is observed in the rest of the positive experiments (paper III, supplementary data). In some of the positive experiments extension of length curves was observed (Fig. 20), which indicates opening of the secondary structures of ssRNA.

Further analysis of the ROI of a representative packaging graph of Fig. 18, A is depicted in Fig. 21. Tether extension during the ROI is shown in Fig. 21, A. Per-section packaged amounts of ssRNA and average packaging velocities are shown in Fig. 21, B and C, respectively. The net amount of packaged ssRNA is much larger in the fast sections (tens of nt), with section-averaged packaging velocities reaching 1.7 nm / s (Fig. 21, C), which is several times larger than the average packaging velocity given by a histogram fit (chapter 5.1.2.1). The maximum velocity in any section reached 4.62 nm / s in certain experiments (paper III, supplementary data).

Packaging velocity also exhibits variation on a longer time scale. This is shown in Fig. 18, which depicts slowdown of the packaging rate 200 - 300 s into the experiment.

Results

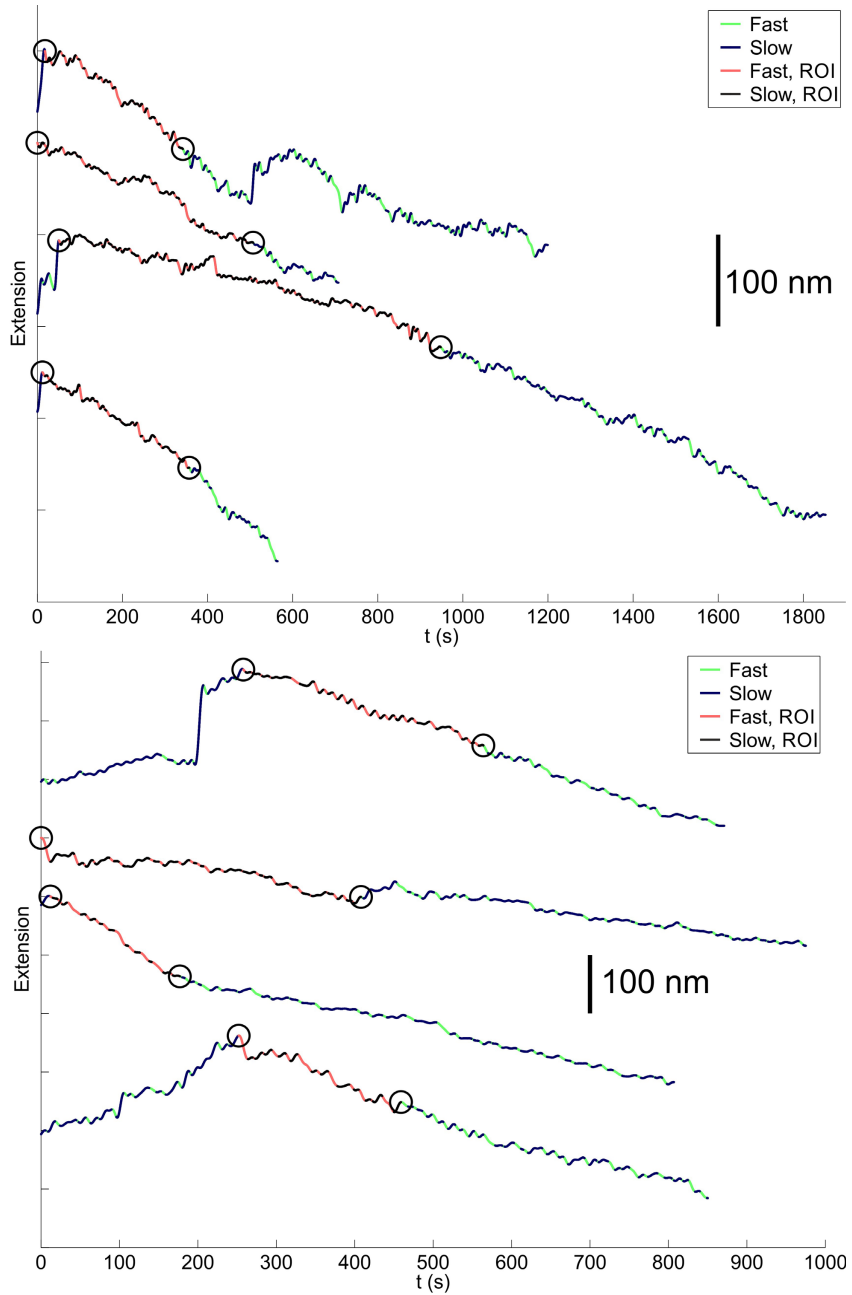


Figure 20 Low-pass filtered ($f_c = 0.1$ Hz) traces of ssRNA packaging of phi6 shown in 8 successful experiments. One unit in y-axis scale is equal to 100 nm (~ 300 nt).

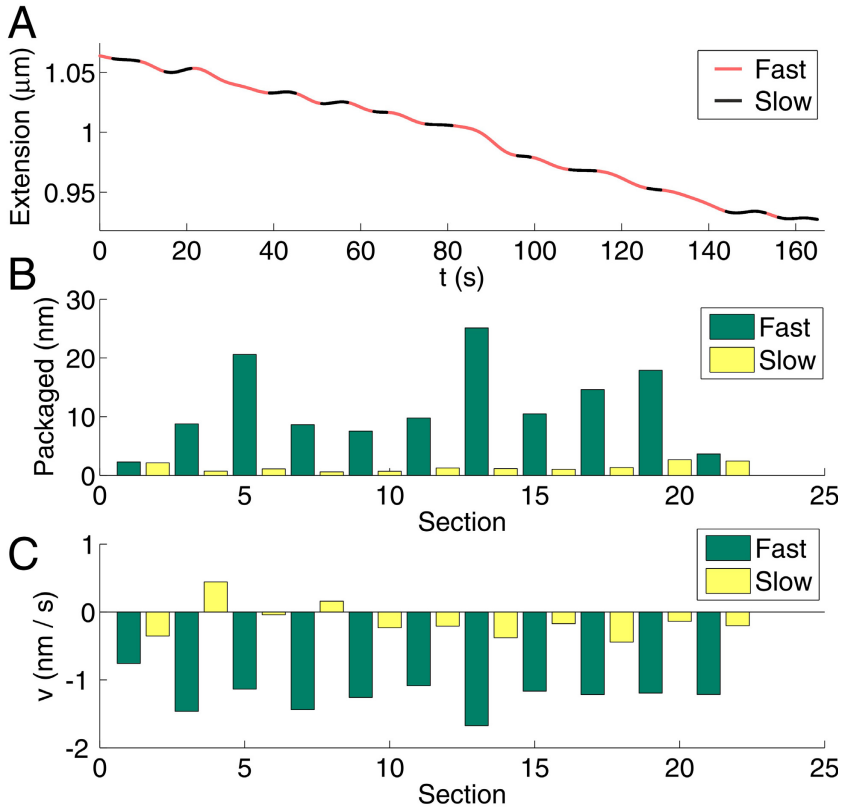


Figure 21 Region of interest during packaging of a representative sample of Fig. 18, A. (A) Low-pass filtered tether length. (B) Amount of packaged ssRNA per section. (C) Average packaging velocity during each section.

6 DISCUSSION

6.1 DNA EJECTION FROM HIS1 IS SUPPRESSED BY OSMOTIC PRESSURE AND INCREASING SALT CONCENTRATION

DNA ejection from His1 was unidirectional, randomly paused, and generally incomplete during these experiments. The ejections were suppressed by external osmotic pressure and by mono- and divalent salts present in the buffer, in agreement with results obtained in dsDNA phage studies [10]. The external osmotic pressure necessary to suppress ejection (~10 atm) agreed qualitatively with the value predicted by the continuum model (Fig. 17, C), although the model is quite sensitive to capsid size, which naturally exhibits variation (Figs. 11 and 17, Appendix A).

The effect of charge screening is clear. In the case of divalent cations (Mg^{2+}), which effectively suppressed ejection already at low concentration. The effect of monovalent sodium chloride was much weaker, which is supported by the fact that the optimal growth condition for *Haloarcula hispanica* (host of His1) occurs at $[Na^+] = 2.5-5.2$ M. Therefore, it seems that even at high NaCl concentrations, His1 retains infectivity, although the number ejections decreases (Fig. 13).

The average maximum ejection velocity ($48.97 \pm 24.48 \mu m / s$, corresponding to 144 ± 72 kbp / s) exceeds that of λ (60 kbp / s) [58], T5 (75 kbp / s) [59, 60], and is similar to that of T7 (140 kbp / s) [61]. The ejection duration is similar to that of λ [58], with single ejections taking 200 – 1200 ms. Variance in the ejection time is caused by random pausing during ejection. This is most likely attributable to friction during ejection caused by e.g. topological friction [62]. Apparent similarity between ejection speeds is unsurprising, since the underlying physical ejection mechanism is basically the same for all of these viruses. Additionally, the exact velocities in the *in vitro* experiments are not easily comparable to actual *in vivo* genome translocation taking place in the natural environment of the host.

DNA ejection from His1 was incomplete resulting in wide distributions of lengths of ejected DNA. Incomplete ejection has also been observed for λ and T5 [14, 58, 60]. This suggests that cellular processes in the host are required to internalize the genome. In the case of SPP1, a host protein binds to the ejected genome, and pulls it into the host cytosol [63]. Similarly, *in vitro* experiments on λ have demonstrated that DNA binding protein can speed up ejection by introducing an additional pulling force [16]. Based on these results it can be hypothesized that His1 may rely on a similar method of infection.

Some viruses such as T5 exhibit pausing during ejection due to nicks in the genome at particular positions along the genome. This is not the case for His1, for which pausing of ejection seems random. It is hypothesized that

incompleteness and pausing during ejection are related to the radical capsid transformation during ejection, and related friction effects. It is unknown whether capsid transformation precedes or follows the ejection process. The capsid adopts an elongated state also in high pH and temperature. Since the current results indicate that the ejection is directional, the transformation of the capsid into a tube is a controlled process, not a random disintegration of the virus. Moreover, due to the directional nature of the ejection, and since cellular processes are likely required to complete internalization of the genome, random pausing during ejection probably plays an insignificant role in the infection process.

6.2 DNA EJECTION FROM HIS1 IS STABLE AS A FUNCTION OF TEMPERATURE AND PH

Extremophilic organisms thrive in a variety of environmental conditions exhibiting for example high salinity and temperature, extreme pH, and varying osmotic pressure [64, 65]. Adaptation to these extreme conditions is supported by the results of paper II, which indicate that DNA ejection is rather insensitive to pH and temperature of the surrounding environment. Ejection is only suppressed at rather low pH (<4.5). At pH 4.5, only 0.1% phosphates of the DNA backbone are protonated (paper II, supplementary data and [66]). Therefore, the effect of pH on the charge density of the phosphate backbone is minimal and should not significantly influence the electrostatic repulsion. This suggests that pH probably affects the capsid more than the DNA. Bulk experiments support the fact that the infectivity of His1 is stable across a wide range of pH (paper II, supplementary data and [21]).

Optimal temperature in terms of the amount of ejected DNA is around 32°C, while the maximum ejection velocity shows a weak, monotonous increase with temperature. The optimal ejection temperature might be related to a phase change in the tightly packaged DNA, similar to what has been described for HSV-1 and λ [25, 26]. Above a certain threshold temperature encapsidated DNA becomes more fluid and the regular hexagonal ordering inside the capsid is disturbed. It is hypothesized that this in turn enhances genome transport to the host cytosol. The theoretical maximum packaging force increases weakly with temperature (Fig. 17). Although there is considerable variation in the maximum packaging force between the capsid size classes, the force always monotonously increases with temperature. While it can be argued that the equilibrium continuum model is unsuitable for describing the out-of-equilibrium ejection process, it at least gives an estimate of the starting energy available for ejection at 100% packaging. Naturally the time-dependent dynamics cannot be extracted from this model without knowing how friction affects the situation. Additionally, recent publications have shown that genome fluidity and capsid elasticity increase with increasing temperature [25, 26]. Therefore, it is hypothesized that His1 may also benefit

from these effects. The optimal growth condition for *Haloarcula hispanica* is pH 6 - 8 and 25 - 50°C [67], which corresponds to the optimal ejection conditions observed in this work. This supports the conclusion that His1 has adapted to the environment of its host in the course of evolution.

6.3 RNA PACKAGING OF PHI6 ALTERNATES BETWEEN FAST AND SLOW VELOCITIES

The efficiency of phi6 during *in vitro* packaging experiments was relatively low, with only 5.4% of positive experiments showing packaging action. This is in line with the efficiency estimate for *in vitro* systems provided by bulk studies (2 - 5%, [31, 37, 51]). The modest number is partly attributable to loss of P4 during purification, which severely affects the efficiency of single molecule experiments [68]. While loss of P4 is the most probable cause of inefficiency in packaging experiments, it should be noted that any part of the multi-component single molecule assay could affect the efficiency. With only part of the P4s present, the random orientation of the PC with respect to the trapped bead may already explain the low number of successful experiments.

The average packaging velocity of phi6 was relatively slow (0.32 nm / s, ~1 nt / s) compared to the estimate obtained from bulk experiments (~33 nt / s, [51]). The average velocity is especially low compared to dsDNA phages (e.g. λ packages at 590 bp / s). The working hypothesis for this apparent slowness is the helicase action of P4. In general, ssRNA in a solution forms elaborate secondary structure, which needs to be opened by P4 before packaging. This is supported by the fact that the average velocities reached 4.62 nm / s (10 nt / s) per section, a value significantly higher than the mean packaging velocity (Paper III, supplementary data). Typical section-average velocities were 1.7 nm / s (~5 nt / s) which is closer to packaging rates reported for phi8 [69]. The intermittent higher velocities can be attributed to packaging of opened parts of the ssRNA. In general, enzymatic reactions of phi6 are slower than that those of dsDNA phages (discussion in paper III). The secondary structure and packaging of ssRNA in the host cytosol is probably different, which would result in differing packaging velocity compared to the single molecule experiments.

The mean packaging velocity does not seem to be sensitive to the clamping force (paper III, supplementary data, Fig. S15), unlike for dsDNA phages [40]. Also packaging velocity did not show significant difference between 1 or 10 mM of ATP. Simple calculation shows that there is order of 10^7 ATP molecules in a $2 \times 2 \times 5 \mu\text{m}^3$ cubical volume surrounding the tether, when ATP concentration is 1 mM. Therefore, even 1 mM of ATP constitutes a saturating concentration and will not be a limiting factor for packaging reaction.

Packaging rate exhibit also longer scale variation, as is apparent from Fig. 18, A. This is unlikely to be related to filling of the capsid, since phi6 PC undergoes several stages of expansion during maturation [37] and only a small

part of the first segment is packaged. However, it is possible that the expansion is initiated by packaging of the whole s^+ -segment [37]. Calculations in paper III (supplementary data) seem to indicate that packaging of ~ 250 nm (735 nt) of ssRNA is enough to fill the center void on the PC, which might be enough to initiate capsid expansion. This length is approximately equal to $1/4$ of the size of the s^+ -segment.

6.4 CONCLUSIONS

Paper I reports on the first results of dsDNA ejection experiments on His1. This is the first single molecule experiment on an archaeal virus. DNA ejection was studied by TIRF microscopy. The main result of paper I was that DNA ejection from His1 can be suppressed with increasing mono- and divalent salt concentration and with polyethylene-glycol induced osmotic pressure. Moreover, it was found that the ejection is unidirectional and generally incomplete, and is randomly paused. The experimental results agreed qualitatively with the predictions provided by continuum theory. Furthermore, these experiments clearly indicated the similarity in DNA ejection between an archaeal virus and dsDNA bacteriophages.

Paper II continues the dsDNA ejection work of paper I. Paper II shows that DNA ejection is suppressed in acidic conditions, when pH was < 4.5 . Above this value ejection is insensitive to pH change. In terms of temperature, ejection is most efficient around 32°C , with minor decline observed for temperatures down to 15°C and for higher temperatures up to 42°C . The average ejection velocity increases slightly with temperature, in qualitative agreement with the change in maximum packaging force as a function of temperature predicted by the continuum theory. The results of paper II support the fact that His1 can infect its host organism across a wide range of environmental conditions, in line with results in the bulk studies reported in the literature. The optimal ejection conditions coincide with the optimal growth conditions of the host, which indicates evolutionary adaptation of His1 to the environment.

Paper III presents the first single molecule packaging experiments on ssRNA packaging of dsRNA phage phi6. The first and shortest of the ssRNA segments (s) of phi6 was packaged in an *in vitro* dual-trap optical tweezers assay. The packaging NTPase P4 packaged the ssRNA segment into an empty procapsid of phi6. Experiments were conducted using constant-force feedback. The main result of paper III shows that while the average packaging velocity is low (0.32 nm / s) compared to previous estimates of the packaging rate, the peak velocity reached 4.62 nm / s (12 nt / s). Packaging takes place in alternating slow and fast sections. It is hypothesized that this is due to the secondary structure of the ssRNA segment which needs to be opened by P4 prior to packaging. Additionally, the average packaging velocity was found to be insensitive to clamping force in the range 1 - 5 pN.

ACKNOWLEDGEMENTS

This thesis is based on research conducted in Electronics Research Laboratory, Department of Physics, University of Helsinki. I acknowledge the heads of the department, Professors Hannu Koskinen and Juhani Keinonen for providing the environment for research.

I acknowledge the Graduate School of Chemical Sensors and Micro-analytical Systems (CHEMSEM) and Ruth and Nils-Erik Stenbäck's foundation for financial support during my research.

I thank my supervisor Professor Edward Hægström for introducing me to the fascinating world of science and never letting me to give up on the highest standards of clarity of thought, whether it was about scientific publication, grant writing or project management in general.

I thank Professors Nynke Dekker and Wouter H. Roos for their efforts in pre-examining my thesis and for their helpful comments. I sincerely thank Professor William M. Gelbart for accepting to be the opponent for my thesis.

I thank my co-authors Professor Dennis Bamford, Docent Minna Poranen and Dr. Maija Pietilä for their collaboration and helpful comments during our research. I am grateful for the opportunity to have been part of their research projects. In particular, Professor Bamford's help in finding the opponent and reviewers for my thesis was invaluable.

I am especially grateful to Dr. Gabija Žiedaitė for her never-ending help and patience during the high and lows of this work. This thesis would not have happened without her support. I am also grateful for her contribution on the biology-part of the work and for reading the thesis manuscript.

I thank Dr. Anders Wallin for his supervision and support during my Master's studies and early graduate work. He taught me a great deal about experimental science. From him I learned bit of a do-it-yourself attitude, which has proven invaluable ever since. I acknowledge his help in commenting on the thesis manuscript.

I thank Docent Ivan Kassamakov for introducing me to the fascinating world of optics and supervision of my earlier studies and for co-authoring many interesting publications later on.

I thank Mr. Juha Aaltonen for his support during my early years in the academic world, and for co-authorship of several papers.

I am grateful to all my friends and colleagues at the Electronics Research Laboratory for the all the lunch and coffee breaks and parties, which made these years much more enjoyable.

And finally my humble thanks for family, especially my parents Riitta and Heikki Hanhijärvi for their tireless support over the years.

Kalle Hanhijärvi, May 2016

REFERENCES

1. Deniz, A.A., S. Mukhopadhyay, and E.A. Lemke, *Single-molecule biophysics: at the interface of biology, physics and chemistry*. Journal of the Royal Society Interface, 2008. **5**(18): p. 15-45.
2. Zlatanova, J. and K. van Holde, *Single-molecule biology: what is it and how does it work?* Molecular cell, 2006. **24**(3): p. 317-329.
3. Knight, A.E., *Single molecule biology*. 2009: Academic Press.
4. Neuman, K.C. and S.M. Block, *Optical trapping*. Review of Scientific Instruments, 2004. **75**(9): p. 2787-2809.
5. Wallin, A.E., A. Salmi, and R. Tuma, *Step length measurement—theory and simulation for tethered bead constant-force single molecule assay*. Biophysical journal, 2007. **93**(3): p. 795-805.
6. Wallin, A.E., H. Ojala, E. Hægström, and R. Tuma, *Stiffer optical tweezers through real-time feedback control*. Applied Physics Letters, 2008. **92**(22): p. 224104.
7. Ojala, H., A. Korsbäck, A.E. Wallin, and E. Hægström, *Optical position clamping with predictive control*. Applied Physics Letters, 2009. **95**(18): p. 181104.
8. Wallin, A.E., H. Ojala, G. Ziedaite, and E. Hægström, *Dual-trap optical tweezers with real-time force clamp control*. Review of Scientific Instruments, 2011. **82**(8): p. 083102.
9. Gell, C., D. Brockwell, and A. Smith, *Handbook of Single Molecule Fluorescence Spectroscopy*. 2006: Oxford University Press.
10. Purohit, P.K., M.M. Inamdar, P.D. Grayson, T.M. Squires, J. Kondev, and R. Phillips, *Forces during bacteriophage DNA packaging and ejection*. Biophysical journal, 2005. **88**(2): p. 851-866.
11. Evilevitch, A., L. Lavelle, C.M. Knobler, E. Raspaud, and W.M. Gelbart, *Osmotic pressure inhibition of DNA ejection from phage*. Proceedings of the National Academy of Sciences of the United States of America, 2003. **100**(16): p. 9292.
12. Panja, D. and I.J. Molineux, *Dynamics of bacteriophage genome ejection in vitro and in vivo*. Physical Biology, 2010. **7**: p. 045006.
13. Vinga, I., C. Baptista, I. Auzat, I. Petipas, R. Lurz, P. Tavares, M.A. Santos, and C. São-José, *Role of bacteriophage SPP1 tail spike protein gp21 on host cell receptor binding and trigger of phage DNA ejection*. Molecular microbiology, 2012. **83**(2): p. 289-303.
14. Evilevitch, A., J.W. Gober, M. Phillips, C.M. Knobler, and W.M. Gelbart, *Measurements of DNA lengths remaining in a viral capsid after osmotically suppressed partial ejection*. Biophysical journal, 2005. **88**(1): p. 751-756.
15. Castelnovo, M. and A. Evilevitch, *DNA ejection from bacteriophage: Towards a general behavior for osmotic-suppression experiments*. The European Physical Journal E: Soft Matter and Biological Physics, 2007. **24**(1): p. 9-18.
16. Löf, D., K. Schillén, B. Jönsson, and A. Evilevitch, *Forces controlling the rate of DNA ejection from phage λ* . Journal of Molecular Biology, 2007. **368**(1): p. 55-65.
17. Speir, J.A. and J.E. Johnson, *Nucleic acid packaging in viruses*. Current opinion in structural biology, 2012. **22**(1): p. 65-71.

18. Pina, M., A. Bize, P. Forterre, and D. Prangishvili, *The archeoviruses*. FEMS microbiology reviews, 2011. **35**(6): p. 1035–1054.
19. Atanasova, N.S., E. Roine, A. Oren, D.H. Bamford, and H.M. Oksanen, *Global network of specific virus–host interactions in hypersaline environments*. Environmental Microbiology, 2012. **14**(2): p. 426-440.
20. Bath, C. and M.L. Dyall-Smith, *His1, an Archaeal Virus of the Fuselloviridae Family That Infects Haloarcula hispanica*. Journal of virology, 1998. **72**(11): p. 9392-9395.
21. Bath, C., T. Cukalac, K. Porter, and M.L. Dyall-Smith, *His1 and His2 are distantly related, spindle-shaped haloviruses belonging to the novel virus group, Salterprovirus*. Virology, 2006. **350**(1): p. 228-239.
22. Pietilä, M.K., N.S. Atanasova, H.M. Oksanen, and D.H. Bamford, *Spindle-shaped viruses infecting halophilic and hyperthermophilic archaea are related*. Environmental Microbiology., 2012. doi:10.1111/1462-2920.12030.
23. Hong, C., M.K. Pietilä, C.J. Fu, M.F. Schmid, D.H. Bamford, and W. Chiu, *Lemon-shaped halo archaeal virus His1 with uniform tail but variable capsid structure*. Proceedings of the National Academy of Sciences, 2015. **112**(8): p. 2449-2454.
24. Grayson, P., *The DNA ejection process in bacteriophage lambda*. 2007, California Institute of Technology.
25. Liu, T., U. Sae-Ueng, D. Li, G.C. Lander, X. Zuo, B. Jönsson, D. Rau, I. Shefer, and A. Evilevitch, *Solid-to-fluid-like DNA transition in viruses facilitates infection*. Proceedings of the National Academy of Sciences, 2014. **111**(41): p. 14675-14680.
26. Sae-Ueng, U., D. Li, X. Zuo, J.B. Huffman, F.L. Homa, D. Rau, and A. Evilevitch, *Solid-to-fluid DNA transition inside HSV-1 capsid close to the temperature of infection*. Nature Chemical Biology, 2014. **10**: p. 861-867.
27. Mertens, P., *The dsRNA viruses*. Virus research, 2004. **101**(1): p. 3-13.
28. Tate, J.E., A.H. Burton, C. Boschi-Pinto, A.D. Steele, J. Duque, and U.D. Parashar, *2008 estimate of worldwide rotavirus-associated mortality in children younger than 5 years before the introduction of universal rotavirus vaccination programmes: a systematic review and meta-analysis*. The Lancet infectious diseases, 2012. **12**(2): p. 136-141.
29. Poranen, M.M., R. Tuma, and D.H. Bamford, *Assembly of double-stranded RNA bacteriophages*. Advances in virus research, 2005. **64**: p. 15-44.
30. Poranen, M.M. and D.H. Bamford, *Assembly of large icosahedral double-stranded RNA viruses*, in *Viral Molecular Machines*. 2012, Springer. p. 379-402.
31. Poranen, M.M., A.O. Paatero, R. Tuma, and D.H. Bamford, *Self-assembly of a viral molecular machine from purified protein and RNA constituents*. Molecular cell, 2001. **7**(4): p. 845-854.
32. Juuti, J.T., D.H. Bamford, R. Tuma, and G.J. Thomas, *Structure and NTPase activity of the RNA-translocating protein (P4) of bacteriophage ϕ 6*. Journal of molecular biology, 1998. **279**(2): p. 347-359.
33. Gottlieb, P., X. Qiao, J. Strassman, M. Frilander, and L. Mindich, *Identification of the packaging regions within the genomic RNA segments of bacteriophage ϕ 6*. Virology, 1994. **200**(1): p. 42-47.
34. Qiao, X., J. Qiao, and L. Mindich, *Analysis of specific binding involved in genomic packaging of the double-stranded-RNA bacteriophage ϕ 6*. Journal of bacteriology, 2003. **185**(21): p. 6409-6414.
35. Pirrtimaa, M.J. and D.H. Bamford, *RNA secondary structures of the bacteriophage ϕ 6 packaging regions*. RNA, 2000. **6**(06): p. 880-889.
36. Huiskonen, J.T., F. de Haas, D. Bubeck, D.H. Bamford, S.D. Fuller, and S.J. Butcher, *Structure of the bacteriophage ϕ 6 nucleocapsid suggests a*

- mechanism for sequential RNA packaging.* Structure, 2006. **14**(6): p. 1039-1048.
37. Nemecek, D., N. Cheng, J. Qiao, L. Mindich, A.C. Steven, and J.B. Heymann, *Stepwise expansion of the bacteriophage $\phi 6$ procapsid: possible packaging intermediates.* Journal of molecular biology, 2011. **414**(2): p. 260-271.
 38. Butcher, S., T. Dokland, P. Ojala, D. Bamford, and S. Fuller, *Intermediates in the assembly pathway of the double-stranded RNA virus $\phi 6$.* The EMBO journal, 1997. **16**(14): p. 4477-4487.
 39. Mindich, L., *Packaging in dsRNA Viruses*, in *Viral Molecular Machines*, R. M.G. and V.B. Rao, Editors. 2012.
 40. Smith, D.E., S.J. Tans, S.B. Smith, S. Grimes, D.L. Anderson, and C. Bustamante, *The bacteriophage $\phi 29$ portal motor can package DNA against a large internal force.* Nature, 2001. **413**(6857): p. 748-752.
 41. Smith, D.E., *Single-molecule studies of viral DNA packaging.* Current opinion in virology, 2011. **1**(2): p. 134-141.
 42. Šiber, A., A.L. Božič, and R. Podgornik, *Energies and pressures in viruses: contribution of nonspecific electrostatic interactions.* Physical chemistry chemical physics, 2012. **14**(11): p. 3746-3765.
 43. Ben-Shaul, A., *Entropy, energy, and bending of DNA in viral capsids.* Biophysical journal, 2013. **104**(10): p. L15-L17.
 44. Ben-Shaul, A., *Reply to the Comment by S. Harvey on "Entropy, Energy, and Bending of DNA in Viral Capsids".* Biophysical journal, 2014. **106**(2): p. 493-496.
 45. Rau, D., B. Lee, and V. Parsegian, *Measurement of the repulsive force between polyelectrolyte molecules in ionic solution: hydration forces between parallel DNA double helices.* Proceedings of the National Academy of Sciences, 1984. **81**(9): p. 2621.
 46. Locker, C.R., S.D. Fuller, and S.C. Harvey, *DNA organization and thermodynamics during viral packing.* Biophysical journal, 2007. **93**(8): p. 2861-2869.
 47. Geggier, S., A. Kotlyar, and A. Vologodskii, *Temperature dependence of DNA persistence length.* Nucleic Acids Research, 2010. **39**(4): p. 1419-1426.
 48. Ojala, H., *Stiffer Optical Tweezers through Real-Time Feedback Control*, in *Department of Physics*. 2007, University of Helsinki.
 49. Ojala, H., *Feedback Controlled Optical Tweezers for Measuring Lambda Exonuclease Activity*, in *Department of Physics*. 2011, University of Helsinki.
 50. Reid, C. and R. Rand, *Probing protein hydration and conformational states in solution.* Biophysical journal, 1997. **72**(3): p. 1022-1030.
 51. Frilander, M. and D.H. Bamford, *In Vitro Packaging of the Single-stranded RNA Genomic Precursors of the Segmented Double-stranded RNA Bacteriophage $\phi 6$: The Three Segments Modulate Each Other's Packaging Efficiency.* Journal of molecular biology, 1995. **246**(3): p. 418-428.
 52. van Dijk, A.A., M. Frilander, and D.H. Bamford, *Differentiation between minus- and plus-strand synthesis: polymerase activity of dsRNA bacteriophage $\phi 6$ in an in vitro packaging and replication system.* Virology, 1995. **211**(1): p. 320-323.
 53. Olkkonen, V.M., P.M. Pekkala, and D.H. Bamford, *Monoclonal antibodies to the major structural proteins of bacteriophage $\phi 6$.* Virology, 1988. **165**(1): p. 317-320.
 54. Ojala, P.M., J.T. Juuti, and D.H. Bamford, *Protein P4 of double-stranded RNA bacteriophage $\phi 6$ is accessible on the nucleocapsid surface: epitope*

- mapping and orientation of the protein. *Journal of virology*, 1993. **67**(5): p. 2879-2886.
55. Canny, J., *A computational approach to edge detection*. *Pattern Analysis and Machine Intelligence*, IEEE Transactions on, 1986(6): p. 679-698.
 56. Abramowitz, M. and I.A. Stegun, *Handbook of mathematical functions: with formulas, graphs, and mathematical tables*. 1964: Courier Corporation.
 57. Bennink, M.L., O.D. Schärer, R. Kanaar, K. Sakata-Sogawa, J.M. Schins, J.S. Kanger, B.G. de Groot, and J. Greve, *Single-molecule manipulation of double-stranded DNA using optical tweezers: Interaction studies of DNA with RecA and YOYO-1*. *Cytometry*, 1999. **36**(3): p. 200-208.
 58. Grayson, P., L. Han, T. Winther, and R. Phillips, *Real-time observations of single bacteriophage λ DNA ejections in vitro*. *Proceedings of the National Academy of Sciences*, 2007. **104**(37): p. 14652.
 59. de Frutos, M., L. Letellier, and E. Raspaud, *DNA ejection from bacteriophage T5: analysis of the kinetics and energetics*. *Biophysical journal*, 2005. **88**(2): p. 1364-1370.
 60. Mangenot, S., M. Hochrein, J. Rädler, and L. Letellier, *Real-time imaging of DNA ejection from single phage particles*. *Current biology*, 2005. **15**(5): p. 430-435.
 61. Kemp, P., M. Gupta, and I.J. Molineux, *Bacteriophage T7 DNA ejection into cells is initiated by an enzyme-like mechanism*. *Molecular microbiology*, 2004. **53**(4): p. 1251-1265.
 62. Marenduzzo, D., C. Micheletti, and E. Orlandini, *Topological friction strongly affects viral DNA ejection*. *Proceedings of the National Academy of Sciences*, 2013. **110**(50): p. 20081-20086.
 63. São-José, C., M. de Frutos, E. Raspaud, M.A. Santos, and P. Tavares, *Pressure built by DNA packing inside virions: enough to drive DNA ejection in vitro, largely insufficient for delivery into the bacterial cytoplasm*. *Journal of molecular biology*, 2007. **374**(2): p. 346-355.
 64. Bowers, K.J., N.M. Mesbah, and J. Wiegel, *Biodiversity of poly-extremophilic bacteria: Does combining the extremes of high salt, alkaline pH and elevated temperature approach a physico-chemical boundary for life*. *Saline Systems*, 2009. **5**(9).
 65. Grant, W., *Life at low water activity*. *Philosophical Transactions of the Royal Society B: Biological Sciences*, 2004. **359**(1448): p. 1249-1267.
 66. Jorge, A.F., R.S. Dias, J.C. Pereira, and A.A. Pais, *DNA condensation by pH-responsive polycations*. *Biomacromolecules*, 2010. **11**(9): p. 2399-2406.
 67. Bowers, K.J. and J. Wiegel, *Temperature and pH optima of extremely halophilic archaea: a mini-review*. *Extremophiles*, 2011. **15**(2): p. 119-128.
 68. Nemecek, D., J.B. Heymann, J. Qiao, L. Mindich, and A.C. Steven, *Cryo-electron tomography of bacteriophage $\phi 6$ procapsids shows random occupancy of the binding sites for RNA polymerase and packaging NTPase*. *Journal of structural biology*, 2010. **171**(3): p. 389-396.
 69. Lisal, J., *Mechanism of RNA Translocation by a Viral Packaging Motor*, in *Institutue of Biotechnology and Department of Biological and Environmental Sciences*. 2006, University of Helsinki: Helsinki.

APPENDIX A: HIS1 CAPSID DIMENSIONS

Table 1. *His1 capsid dimensions deduced from [23]. All values are in nanometers.*

	Class I	Class II	Class III	Class IV	Tube
Geometry	Ellipsoid	Ellipsoid	Ellipsoid	Ellipsoid	Cylinder, spherical end-caps
Internal width	55.64	57.53	59.44	59.16	116.00
Internal height	28.63	28.69	30.31	29.43	15.00
Half-width	27.82	28.77	29.72	29.58	
Half-height	14.32	14.35	15.16	14.72	
Volume nm ³	23883.62	24803.93	28594.62	26837.69	24033.18
Packaging density	0.65	0.62	0.54	0.58	0.64

APPENDIX B: OPTICAL PARTS OF THE TIRF MICROSCOPE

Table 2. *Table of TIRF microscope components. Component designations refer to Fig. 4.*

Component	Manufacturer	Description	Model
OBJ	Nikon	TIRF objective (oil imm.)	CFI Apo TIRF 100X, N=1.49
EMCCD	Andor	EMCCD camera	iXon DU-897
L1	Thorlabs	Plano-concave lens	LC1715-A, f = -50 mm
L2	Thorlabs	Plano-convex lens	LA1608-A f = 75 mm
T6	Thorlabs	Galilean beam expander	BE20M-A, 20×
L5	Thorlabs	Plano-convex lens	LA1725-A, f = 400 mm
D1	Semrock	Dichroic mirror	Dich495-Di03
S1	Ludl	Shutter	99A360
F2	Semrock	Optical band-pass filter	520/35-23
HWP	Thorlabs	Half-wave-plate	WPH05M-488
488	Coherent	Excitation laser	Sapphire 488, 50 mW